TRIBHUVAN UNIVERSITY

INSTITUTE OF ENGINEERING

PULCHOWK CAMPUS

THESIS NO: 079/MSPSE/014

Impact Analysis of Electric Vehicle (EV) Charging on Medium Voltage Distribution Feeder Network (Sanepa Feeder)

by

Om Bikram Shah

A THESIS

SUBMITTED TO THE DEPARTMENT OF ELECTRICAL ENGINEERING IN PARTIAL FULFILLMENT OF THE REQUIREMENT FOR THE DEGREE OF MASTER OF SCIENCE IN POWER SYSTEM ENGINEERING

DEPARTMENT OF ELECTRICAL ENGINEERING

PULCHOWK CAMPUS

LALITPUR, NEPAL

DECEMBER, 2025

Impact Analysis of Electric Vehicle (EV) Charging on Medium Voltage Distribution Feeder Network (Sanepa Feeder)

By

Om Bikram Shah

PUL079MSPSE014

Thesis Supervisor

Dr. Bishal Silwal

MSc. Coordinator, Associate Professor, Department of Electrical Engineering Pulchowk Campus, IOE, Tribhuvan University, Nepal

A thesis submitted to the Department of Electrical Engineering in partial fulfilment of the requirements for the Degree of Master in Power System Engineering

Department of Electrical Engineering

Institute of Engineering, Pulchowk Campus, Tribhuvan University

Lalitpur, Nepal

December, 2025

COPYRIGHT

Accredited by University Grants Commission (UGC) Nepal 2020

त्रिभुवन विश्वविद्यालय
TRIBHUVAN UNIVERSITY
इन्जिनियरिङ्ग अध्ययन संस्थान
INSTITUTE OF ENGINEERING
पुल्चोक क्याम्पस
PULCHOWK CAMPUS
DEPARTMENT OF ELECTRICAL ENGINEERING
Pulchowk, Lalitpur

CERTIFICATE OF APPROVAL

The undersigned certify that they have read, and recommended to the Institute of Engineering for acceptance, a thesis entitled ***"Impact Analysis of Electric Vehicle (EV) Charging on Medium Voltage Distribution Feeder Network (Sanepa Feeder)"*** submitted by **Mr. Om Bikram Shah** in partial fulfillment of the requirements for the degree of **Masters of Science in Power System Engineering**.

.....

Asst. Prof. Dr. Bishal Silwal
Program Coordinator
MSc. in Power System Engineering
Department of Electrical Engineering
Pulchowk Campus, Lalitpur
(Supervisor)

.....

Assoc. Prof. Dr. Shailendra Kumar Jha
Department of Electrical and Electronics Engineering,
School of Engineering, KU
Dhulikhel, Nepal
(External Examiner)

.....

Asst. Prof. Dr. Bishal Silwal
Program Coordinator
MSc. in Power System Engineering
Department of Electrical Engineering
Pulchowk Campus, Lalitpur

.....

Assoc. Prof. Jeetendra Chaudhary
Head of Department
Department of Electrical Engineering
Pulchowk Campus, Lalitpur

December, 2025

ACKNOWLEDGEMENT

I would like to express my gratitude to all those who have contributed to the successful completion of this thesis entitled *"Impact Analysis of Electric Vehicle (EV) Charging on Medium Voltage Distribution Feeder Network (Sanepa Feeder)"*. This challenging and rewarding journey had been made possible with the constant collaboration, guidance and encouragement from several people and institutions.

First of all, I like to thanks my supervisor Dr. Bishal Silwal, Assistant Professor and MSc. Coordinator, Department of Electrical Engineering, Pulchowk Campus, for his support and guidance from very beginning of this thesis. His patience and encouragement throughout this work have been a great motivation for completion of my work. His expertise in power systems and thoughtful supervision has been instrumental in shaping this work to its present form.

The advice, encouragement, academic guidance and technical support required during my thesis work was constantly provided by the Head of the Electrical Engineering Department and all the faculty members of the Institute of Engineering, Pulchowk Campus. So, I like to sincerely thanks all of them with my heart.

Special thanks to the Thapathali Switching Station, Pulchowk Distribution Control System (DCS), Teku Substation, and Baneshwor NEA Office for their contribution in providing invaluable data which make the modelling of Sanepa feeder replicated realistically. I would also like to acknowledge Sajha Yatayat, BYD, MG, and Hyundai charging stations for allowing access to their charging infrastructure and providing operational data which helps to modelled the EV chargers representing the algorithm used by most of the commercial chargers nowadays.

Furthermore, I am thankful to the Department of Mechanical Engineering, Kathmandu University, for hosting the *4th University Scholar Conference 2025: ENGINEERING, INNOVATION AND ADVANCEMENTS*, which offered valuable exposure and the opportunity to present and refine this research.

Finally, I want to give deep appreciation to my friends and family for their constant motivation, patience, and support. Their encouragement reflected as my strength throughout this academic journey. This thesis stands as a reflection of the collective effort and support of everyone mentioned above, and I am truly grateful for their contributions to my academic and personal growth.

ABSTRACT

The rapid uptake of EVs has increased the demand for fast charging facilities, which challenges medium voltage distribution feeders in terms of power quality. The present work discusses the impacts of several public and private EV charging stations on the Sanepa feeder, a representative medium voltage feeder in the Lalitpur distribution network. Power factor degradation and harmonic distortion caused by nonlinear EV chargers at significant public and private charging stations, such as BYD, MG, Hyundai, and NEA charging centers, and Sajha Yatayat were studied. Nine operational scenarios were simulated from single EV charging station operation to simultaneous operation of all five stations. According to the results, in the scenario when all stations are operational, the maximum THD at some buses is up to 3.85% at realistic maximum ev penetration case, while the minimum PF falls down to 0.6 at the farther end, Labim Mall. There has been significant deterioration in power quality in the distribution network. Additional analysis has been performed to determine the maximum number of chargers that can be simultaneously employed at each location without violating the 5% THD limits recommended by IEEE standards. The analysis revealed that even the full-capacity simultaneous operation of chargers at the BYD, Hyundai, and MG stations has negligible impact, while the simultaneous full-capacity operation of chargers at the NEA and Sajha stations increases the THD to 4.26%. Further analysis was conducted at different locations in the Sanepa feeder to assess the network's hosting capacity for EV chargers. The study identified the maximum number of additional EV chargers that could be accommodated at each site within the existing grid without breach of the IEEE-recommended 5% THD limit, without the violation of acceptable power factor conditions at those sites. These results have provided location-specific guidelines for controlled EV charging growth and grid planning in an urban medium voltage feeder. The impact of the entire charging network has been assessed, and operational limits have been set to define the reliable integration of EV chargers at each site, thus giving location-based recommendations for controlled expansion and grid planning. All system modeling and simulations are performed in the MATLAB/Simulink environment.

Keywords — Electric vehicle charging, Power quality, Harmonics, Distribution feeder

TABLE OF CONTENTS

LIST OF TABLES

LIST OF FIGURES

LIST OF ABBREVIATIONS

EV	Electric Vehicle
EVCS	Electric Vehicle Charging Station
BEV	Battery Electric Vehicle
ICEV	Internal Combustion Engine Vehicle
IEA	International Energy Agency
PF	Power Factor
THD	Total Harmonic Distortion
IEEE	Institute of Electrical and Electronics Engineers
FFT	Fast Fourier Transform
DFT	Discrete Fourier Transform
PFC	Power Factor Correction
SOC	State of Charge
CC	Constant Current
CV	Constant Voltage
RMS	Root Mean Square
PU	Per Unit
MATLAB	Matrix Laboratory

CHAPTER 1: INTRODUCTION

1.1 Background

With the increasing concept of clean and green energy, vehicles using fuel are slowly decreasing, and electric vehicle (EVs) are increasing rapidly. Since they don't emit any direct pollutants, EVs has a considerably lesser detrimental effect on the environment and public health than internal combustion engine vehicles (ICEVs). The decline in air quality is primarily driven by emissions from vehicle exhausts, particularly nitrogen oxides (NOx) and particulate matter (PM). Battery electric vehicles (BEVs) cut PM emissions by a factor of four and NOx emissions by a factor of twenty when seen from a well-to-wheel perspective. Because of this, EVs are essential for slowing down climate change, improving public health, and inspiring the growth of intelligent, sustainable urban regions [1].

In recent years, popularity of Electric vehicles as a means of transportation is increasing rapidly which includes both electric cars and bikes. EVs are considered as environmentally sustainable and eco-friendly means compared to IC engine vehicles which utilize petroleum fuels. With popularity, EVs use grows by more than 50% by the year 2024. According to the International Energy Agency (IEA), the global stock of EVs has seen substantial growth over the past decade, reaching 10 million in 2022 and projected to rise to 30 million by 2030. Recent progress in EV charging technology has been remarkable. The industry is increasingly embracing innovations like 350kW DC fast chargers and wireless charging systems, both of which are emerging as key developments in the field [1].

Electric vehicles operate with rechargeable batteries which are charged drawing electric power from the utility grids. To enable rapid charging, electric vehicle charging stations (EVCS) incorporate high-speed power converters, sophisticated filtering networks, and advanced control schemes—all of which introduces non-linearity in the grid. With the increment of EV market, the expansion of reliable, efficient and safe charging infrastructure would be a backbone for its wider adoption. However, current charging networks around the world are not evenly developed and often cannot meet the growing demand. This study also reviews the global and local status of charging infrastructure development, identifies the current challenges and opportunities, and

proposes relevant recommendations for improvement. This study expects to provide meaningful insights and directions to policy makers, industrial professionals and researchers which can be beneficial for continued advancement and growth of the Electric Vehicle (EV) sector.

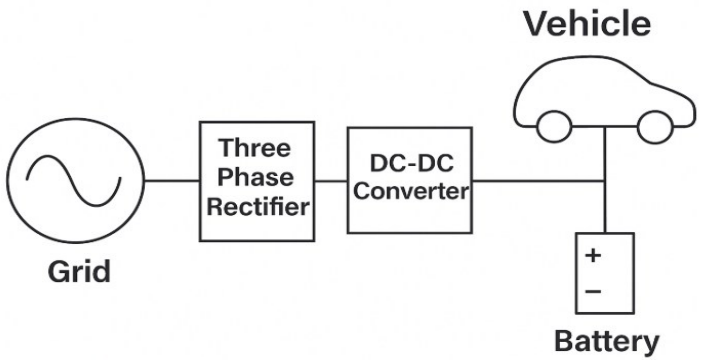

Figure 1. 1 Electric Vehicle Connection to Grid

1.1.1 Evolution of EV charging infrastructure

The development of EV charging stations has progressed in multiple phases:

- Early Stage (2000s-2010s): Initial charging infrastructure focused on slow AC charging for home and commercial applications.
- Expansion (2010s-2020s): Adoption of fast DC chargers (such as CCS, CHAdeMO, GBT, and Tesla Superchargers)
- Smart Charging & Vehicle to Grid (2020s and beyond): Integration of renewable energy, battery storage, and V2G capabilities to enhance grid stability and efficiency.

1.1.2 Components of an EV charging station

The power supply and regulation of electricity from grid to the EVs is handled by components mentioned below.

A. Power Source

Most of the charging stations are connected to the grid which might be single phase or three phase depending upon the nature of its use as for residential or commercial purposes respectively. With the aim to reduce carbon emissions, renewable energy sources like PV

are being integrated as primary or supplementary power source to the EVs. Solar photovoltaic (PV) systems are the most commonly used means which are constructed on stations roofs or nearby lands to convert sunlight into the electrical energy. Thus, produced electricity is immediately used or stored in battery energy storage systems (BESS) for later use. According to research published in Renewable and Sustainable Energy Reviews, solar-powered charging reduces the dependency on grid, increases resilience and also reduces the long-term operational costs. Though less common, wind energy is also used in rural and high-wind areas which integration with BESS can improve reliability. Additionally, smart grid integration and energy management systems allow for demand response and optimized energy flow between renewable sources, the grid, and EVs. This shift toward renewables in EV infrastructure supports global goals for decarbonization and energy independence. Batteries can be integrated to support peak demand and enable vehicle-to-grid operations.

B. Transformer

It steps the high-voltage grid power (33kV or 11kV) to charging voltage level (400V or 230V). This 400V is utilized by three phase chargers which is ideally for commercial and public EV charging stations using high-power chargers. Additionally, transformer enhance the safety and reliability as it isolates the charging stations from high-voltage grid. The impedance of transformer winding also suppresses the high frequency harmonics greater than 2kHZ.

C. Power Electronics (AC/DC Converters & Inverters)

An AC/DC rectifier converts alternating current (AC) from the grid into direct current (DC), which is then either increased or decreased by a Buck/Boost converter to adjust the DC voltage level to match the requirements of the battery. In fast charging, DC fast chargers with high-power rectifiers (rated from 50 kW to 350 kW) are used to directly supply DC to the EV. Some chargers may include power factor correction circuits to improve efficiency and reduce harmonic distortion.

- AC Chargers (On-board or Off-board): Directly supply AC power, and the EV's onboard charger (OBC) converts it to DC.

- DC Fast Chargers (Off-board): Convert AC to DC externally and directly charge the EV battery, allowing much faster charging.
- Bidirectional Converters (for V2G and V2H applications): Allow power flow from EV to grid (V2G).

1.1.3 Electric Vehicle Market Growth in Nepal (2020–2025)

Nepal has seen a dramatic surge in EV imports and adoption over the past five years. According to *The Kathmandu Post* and other national reports:

- In FY 2024–25, about 10,036 electric vehicles were imported in the first nine months, compared to 6,268 internal combustion engine (ICE) vehicles [Kathmandu Post, 2025].
- For the fiscal year ending July 16, 2025, the growth of EVs is about 73% of all four-wheeled passenger vehicle imports in Nepal, marking a historical shift toward electrified mobility [Kathmandu Post, 2025].
- The adoption rate of EVs in Nepal is among the highest globally, as new EV imports rose from *just a few hundred units per year as recently as 2020* to thousands by 2024 [The Guardian, 2024; Nepal Economic Forum, 2024].
- Policy incentives like customs and VAT concessions have boosted the Use of EVS rather than ICE vehicles [Kathmandu Post, 2024].
- Among total registrations of EVs in Nepal, two-wheelers make about 85% of new vehicles, suggesting the potential growth of EV market. [Nepal Economic Forum, 2025].

Overall, Nepal is moving towards cleaner and sustainable means of transport driven by both government support and public demand.

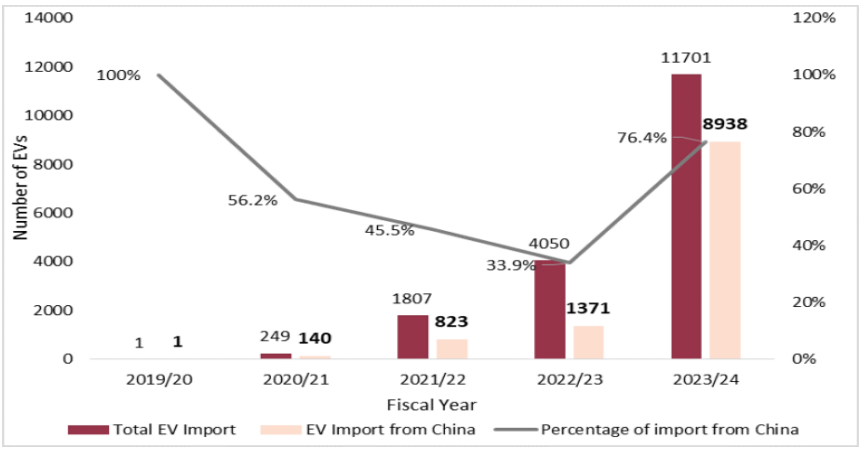

Figure 1. 2 Electric Vehicle Import Growth in Nepal

(Source: The Kathmandu Post, The Guardian, Nepal Economic Forum)

1.1.4 EV charging station in Nepal

NEA presently operates 62 charging stations across Nepal and has 30 CCS-2/Gb/T-142 kW-rated stations. NEA has sanctioned a further 750 at 105.32 MW out of which 60 MW is already installed. The cumulative EV charging capacity including private stations, installed in Nepal to date is 78.8 MW and catering to an average power supply of 322,300 kWh per day. NEA charging stations receive support from the nearest transformer and are categorized as NEA Charging Station Customer Group whereas all other privately owned charging stations are categorized under different customer groups.

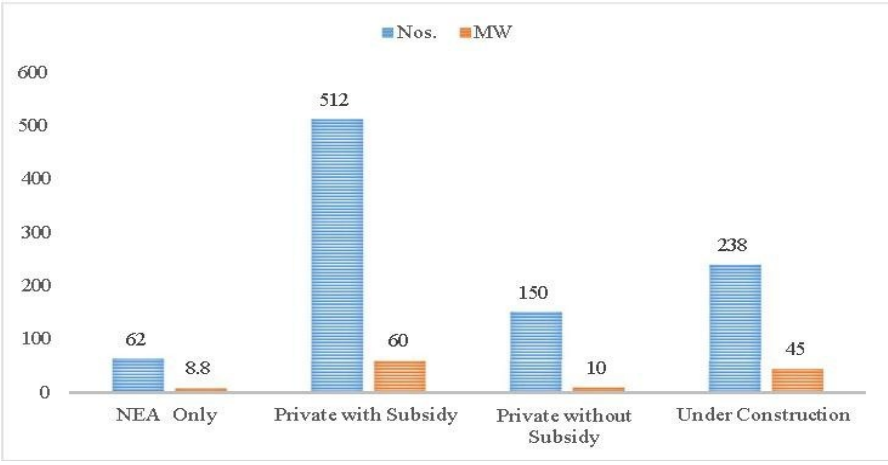

Figure 1. 3 Status of EV Charging Stations in Nepal

1.2 Problem Statement

Integration of charging infrastructure into the distribution feeder is very crucial for power quality with the rapid adoption of electric vehicles in Nepal. The Sanepa feeder caters to residential and commercial loads in Lalitpur and is presently operating several three-phase DC fast chargers without major voltage or current distortion. These use AC-DC and DC-DC converters that create non-linear loads and thereby inject harmonics of the order of 5th, 7th, 11th, and 13th into the system, which can increase transformer heating and losses, reducing efficiency.

Presently, THD lies within the IEEE 519 limit of 5%; however, additional chargers might increase it further and lower the power factor. The harmonic profile and thereby the capacity of the feeder for more electric vehicle chargers is assessed through this study, which will guide the development of mitigation strategies in the future, such as an Active Power Filter.

1.3 Objectives

Main Objective:

- To analyze the impact of existing Ev charging stations on Sanepa feeder by evaluating THD (Voltage and Current), power factor degradation, voltage profile, total and harmonic losses.

Specific Objectives:

- To develop the realistic model of Sanepa feeder using collected data in MATLAB/Simulink.
- To model the EV chargers on Sanepa feeder using CC/CV algorithm to switch the mode of charging based on SOC of battery (i.e. 80%)
- To simulate the feeder performance under various scenarios representing different EV penetration levels during the 24 hrs time frame.
- To assess the voltage profile, power factor, losses, and THD at near and far-end buses.

- To determine the maximum number of additional EVs that can be integrated into the existing feeder without violating IEEE 519 limits.

1.4 Scope of Thesis

The research presented here focuses on assessing various impacts of the already-existing and potential EV charging stations on the Sanepa medium-voltage feeder in Kathmandu Valley. In this respect, Sanepa feeder with various operational EV chargers on feeder are modelled in MATLAB/Simulink to analyse the impact on power quality factors, including voltage profile, power factor, losses and THD. EV chargers are modelled as three phase fast DC chargers switching CC/CV mode depending on SOC of battery (80%). The CC/CV algorithm is employed by most of the commercial chargers nowadays.

This work evaluates various electric vehicle penetration levels in different daily scenarios-morning, day, evening, and night-and calculates the maximum number of additional chargers that can be added without exceeding the IEEE 519 limit of 5% THD or violating acceptable PF conditions. Since the THD levels remain with acceptable limits, controlled integration of additional chargers is done rather than using other mitigation techniques.

The findings provide utilities, planners, and policymakers with guidance on feeder hosting capacity and location-specific EV expansion. These results will also help in future grid planning, designing new EV stations, and integrating compensation devices like STATCOMs or active filters if higher EV penetration increases harmonics or reduces PF. This framework can be applied to similar urban distribution networks to facilitate sustainable EV adoption with maintained grid stability.

1.5 Limitations of thesis

While this study provides a comprehensive assessment of EV integration on the Sanepa medium-voltage feeder, several limitations should be noted:

- The analysis is focused strictly to Sanepa feeder only without considering the impact of EVs that can hamper the rest feeder in Kathmandu valley feeders' network in terms of power quality.

- Power quality issues, such as voltage sags, swells, flickers, and frequency variations, are not analysed in this study.
- Single-phase EVs, such as electric two-wheelers (bikes and scooters) and three-wheelers (tempos), which are increasing in number in urban and residential areas, are not modelled due to insufficient data regarding their charging patterns, number of vehicles, and locations.
- Future EV growth and extreme charging scenarios beyond the currently available data are not included, which may limit the analysis under peak or high-penetration conditions.
- Load diversity and stochastic EV arrival patterns are simplified; real-world variability in charging times and loads is not fully captured.
- Static power quality analysis is performed; dynamic effects, such as transient response or grid interactions under rapid charging events, are not considered.
- Harmonic mitigation techniques (such as ASPF, or advanced control strategies) are not employed in the current study which might be necessary to maintain the power quality limits with additional EVS on feeder with existing infrastructure.

1.6 Thesis Organization

This dissertation is organized into six chapters. This section gives a brief outline of each chapter and the contents of each.

Chapter 1: It introduces the study, providing the background of EV adoption, the problem statement, main and specific objectives, scope of the thesis, and limitations of the work.

Chapter 2: It presents the literature review, including EV impacts on feeder, problem with EV integration in feeder performance, EV charger modelling, Harmonics mitigation techniques, PWM control and the EV growth trend in Nepal (2020–2025).

Chapter 3: It describes the research methodology, including data collection, Sanepa feeder and EV charger CC-CV modeling, simulation scenarios, and performance metrics such as voltage, PF, losses, and THD.

Chapter 4: It presents the case study results of voltage, PF, losses, THD, and maximum additional EV chargers within IEEE limits.

Chapter 5: It contains conclusions and key findings, recommendations for future EV integration and mitigation of power quality.

Chapter 6: It lists references, including scholarly articles, IEEE standards, reports and news sources.

CHAPTER 2: LITERATURE REVIEW

2.1 Overview

Distribution feeders are critical components of electrical distribution systems that transport power from substations to end users. They consist of overhead and underground conductors, transformers, circuit breakers, and protection devices. The design and operation of distribution feeders aim to ensure reliable and efficient power delivery while minimizing losses and maintaining power quality.

Contemporary distribution networks are advancing with the incorporation of renewable energy sources (RES), including photovoltaic (PV) and wind energy systems. The IRENA's worldwide plan stated that renewable energy consumption will increase from 20% to 40% till 2050 and the output from renewable energy sources will increase by two-third. Besides 2050 the solar generation and wind energy production will donate three times as much as from 20% to 60%. Different actions have been brought in front for effective implementation and to prevent rapid extension of ICEVs [2]. Moreover, as the electricity demand from EVs can be rapidly introduced or withdrawn from the power grid, electrical infrastructure such as power generation units and transformer systems become particularly susceptible to fluctuations in system frequency. Hence, in response to the rapid rise in EV adoption, the power grid requires substantial development to keep pace. Strong government incentives, strategic placement of generation units near EV chargers, and efficient use of EV batteries and power electronics are key to meeting rising energy demand while managing infrastructure costs

Microgrids are more complex and nonlinear than conventional plants due to distributed energy sources, diverse loads, and energy conversion devices. Power quality directly affects safety and efficiency, and widespread EV adoption can greatly increase residential power demand—charging one EV is roughly equal to two households. [3].

2.2 Harmonics in Power Systems

Harmonics are non-sinusoidal components in electrical waveforms that arise due to nonlinear loads such as power electronic devices, transformers, and fluorescent lighting. These harmonics

distort voltage and current waveforms, leading to reduced power quality, increased losses, overheating of equipment, and malfunction of sensitive electronic devices.

Common sources of harmonics in distribution feeders include:

- Power electronic converters (e.g., inverters, rectifiers)
- Adjustable speed drives (ASDs)
- Uninterruptible power supplies (UPS)
- Nonlinear industrial loads

2.3 Effects of Harmonic Distortions in Power Systems:

Harmonics are generally undesirable in electrical power systems, as they adversely affect both the equipment and the overall operation of the system. Resonance in a power system network can be generated via harmonics [4].

A. Resonance

Power factor correction capacitors can resonate with system harmonics to cause excessive currents and possible damage. Parallel resonances magnify harmonic voltages and currents because of high impedance, whereas series resonances result in high capacitor currents with lower harmonic voltages. Furthermore, interactions in converter controls produce nonintegral composite resonant frequencies that further affect the capacitors.

B. Poor Damping

When harmonics are present, a slight negative impedance or resistance may be added by SMPS or variable speed drive motors. As voltage increases, it lowers current, which lowers the system's damping or broadband energy absorption capacity. Unwanted variations in damping level affect the degree to which certain electrical equipment operate, particularly various measuring and regulating devices.

C. Effects on Rotating Machine

Harmonic loss: Increased losses in the stator/rotor windings and laminated cores due to eddy currents, skin effect, and higher copper/core losses result in the heating and reduction of efficiency.

Harmonic torque: Positive sequence harmonics aid shaft rotation; negative sequence harmonics oppose rotation.

Speed torque characteristics: Harmonics change magnetic forces, which have an impact on the overall speed and torque characteristics.

Cogging: Motor cannot reach normal operating speed when stuck at low-frequency operating point..

Voltage stress: Harmonic voltages contribute to greater stress on insulating materials.

D. Impact on transformers

RMS Current: Due to the increase in current harmonics distortion in the transformer it results in a higher RMS peak value, which leads to the increased heating within the transformer.

Core loss: Both the eddy current loss and hysteresis current losses in the laminations are increased due to harmonic voltage. The supply voltage's harmonics, the magnetic circuit, and the core material’s design specifications all affect how substantially core loss occurs.

Copper loss: Harmonic currents lead to an increase in copper losses. The loss is primarily determined by load's harmonics and the winding's effective AC resistance. Copper loss increases temperature which creates hot spots in that transformer.

Stress: The stresses of the insulation increase due to the voltage harmonics.

Core vibration: Small core vibrations are exacerbated by harmonics of current and voltage.

Saturation problem: Additional harmonic voltage might occasionally end up in core saturation.

E. Effects on the Transmission System

Skin effect and Proximity effect: This type of effects is frequency-dependent, and the presence of harmonics amplifies them. Consequently, the effective AC resistance rises when harmonics are present.

Loss: The presence of additional harmonic currents leads to increased copper losses in the transmission system and diminishes its overall power transmission capacity. The formula to calculate copper loss is expressed by $\sum^{\alpha}{}_{n=2} In^2 Rn$, where I_n represents the nth harmonic current, and R_n is the system resistance at that specific harmonic frequency.

Voltage drops: Harmonic currents lead to voltage drops across circuit impedances. Weak systems with high impedance have larger disturbances, while stiff systems with low impedance have minimal voltage drops.

Dielectric stress: Harmonic voltages increase the dielectric stress on transmission cables, proportionally to the peak applied voltage. The insulation strength is reduced, cable life is shortened, and the risk of faults and maintenance costs increased.

Corona: Harmonics affect the peak-to-peak voltage, influencing the initiation and extinction of the corona discharge. Higher harmonic voltages increase the overall peak voltage that may alter corona behaviour in transmission lines.

F. Effects on Capacitor Banks

Issues related to distortion usually manifest initially on the power bank of the capacitor. Under conditions of peak voltage harmonics, the capacitor bank may enter a state of resonance, during which the flow of current through the bank becomes significantly large, resonance condition is especially significant when dominant monotonic harmonics are present, with the eleventh harmonic being notably affected which becomes superimposed on the fundamental frequency, thereby impacting the overall behaviour of the capacitor bank. As a result, the root mean square (RMS) current during resonance often exceeds the capacitor's rated RMS current, potentially compromising its performance and operational lifespan. The IEEE Standard for Shunt Power Capacitors (IEEE Standard 18-2002) [5]. It outlines the following continuous capacitor ratings:

- 135% of the total KVAR.

- 110% of the rated RMS voltage value, along with the harmonics once the transient effects have dissipated.
- The capacitor is subjected to a voltage level reaching 120% of the nominal value, inclusive of harmonic content.

Among the harmonic components, the fifth and seventh harmonics are most prominent in affecting the capacitor. The distorted voltage waveform consists of 4% fifth harmonic and 3% seventh harmonic components. As a result, this leads to a 20% fifth harmonic current and a 21% seventh harmonic current flowing through the capacitor. Despite these distortions, all resulting harmonic values remain within acceptable standard limits under the given conditions.

G. Effect on Measuring Instruments

Utilities measure the consumption of power in their distribution systems by total energy consumed and peak demand. Large corporate customers are usually billed for both energy and demand, although residential users usually pay only for the amount of energy used. The price for the power will be a function of kWh consumed, and the KVA rate is determined by the distributor's need to maintain sufficient capacity, typically derived from the maximum demand over 15–30 minutes. Watt-hour devices, associated with apparent power meters, log energy use in intervals and reset at each cycle.

Harmonics from nonlinear loads affect the accuracy of KVA meters. Conventional induction meter theory is based upon rotor speed being proportional to energy transfer, but the usual disc-type magnetic meters commonly under-record at harmonic frequencies. Linear loads include harmonic energy but nonlinear devices can inject harmonics back to the source. Since meters are calibrated for sinusoidal AC, harmonics introduce errors in measurement; the error sign depends upon the magnitude and direction of harmonic power. Harmonic voltages and currents degrade a meter's capability for accurate measurement of fundamental frequency power.

H. Effect on Power System Protection

Protective relays operational qualities are deteriorated by harmonics. The design parameters along with operating principles determine how harmonics affect the relay.

Circuit breakers and fuse's ability to cause interruptions is impacted by current harmonic distortion. Due to more heating in the solenoid, harmonics cause increased di/dt at zero crossing point , and the thermal magnetic breakers' current detection capability modifies the trip point.

These downsides increase the cost of industrial manufacturing and other commercial events, due to the degrade seen in overall quality of the product material and decreased production [4].

I. Effect on Consumer Equipment

Television Receivers: The change in picture size and brightness of the TV set is influenced by harmonics. Also, the amplitude modulation of the fundamental frequency is altered due to harmonics [4]. As, an example with introduction of 0.5% of interharmonic this leads to periodic amplification and decrement of the image of CRT screen.

In lighting systems like fluorescent and mercury arc lamps, capacitors combined with the inductive elements of the ballast and circuitry form a resonant network that produces a specific resonant frequency. This resonance can lead to excessive thermal stress, ultimately causing operational failure of the components. Additionally, harmonic voltage distortion contributes to the generation of audible noise, further impacting the system's performance and reliability.

2.4 Harmonic Analysis Techniques

Harmonic analysis involves measuring, modelling and assessing the impact of harmonics on power systems. Various techniques are used for harmonic analysis, including:

I. Fourier Transform-Based Methods:

This methodology is one of the versatile Frequency Domain Analysis that is employed for harmonics. The wide application of Digital Signal Processor and microcomputer have introduced the algorithms such as FFT and DFT [6]. These algorithms have accurate precision and can be employed to detect the selective order harmonics, but delay in a complete cycle is inevitable. Also, the actual meaning is not clear by the conversion between frequency and time domain.

It is the most powerful tool in mathematics, for converting a time-domain signal into the frequency domain (t), the Fourier Transform $\{(t)\}$ is defined as [7]:

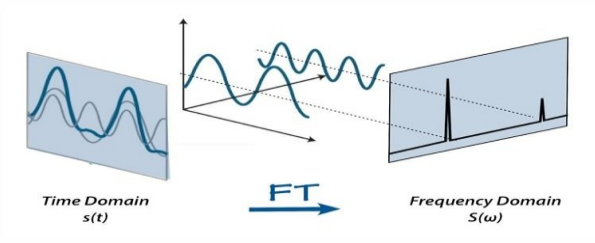

Figure 2. 1 Conversion from time domain to frequency domain for a continuous-time signal

II. Discrete Fourier Transform:

Discrete signals are used in most instances of electrical parameter measurements. The Fourier transform (FT) is altered to switch from the Discrete Fourier transform (DFT) in order to handle such discrete signals. For a sequence $[n]$ of length N, where n=0,1, 2.…..,,$N-1$, the DFT $X[k]$ is defined as [4]:

$[k] = \sum_{n=0}^{N,-1} x\,(n) e^{-j\frac{2\Pi}{N}kn}$, k =0,1, 2……, N-1 (2.1)

Where, N represents the total number of samples within one period.

III. Fast Fourier Transform (FFT)

The primary disadvantage of DFT is that it takes considerable time to work out for big values of N. The Discrete Fourier transform can be computed effectively using FFT technique. The matrix required for multiplication in the Discrete Fourier Transform (DFT) is decomposed into several simpler forms using the Fast Fourier Transform (FFT). This shortens both the execution time and the multiplication procedure [6].

IV. Wavelet Transform (WT)

It offers time-frequency localization, making it suitable for non-stationary harmonic analysis.

V. Artificial Intelligence (AI) based methods

Deep learning and machine learning techniques are increasingly applied for harmonic pattern recognition and classification.

VI. MEMO-ESPRIT (Multiple Signal Classification and Estimation of Signal Parameters via Rotational Invariance Techniques)

An advanced method for harmonic and inter-harmonic estimation with high resolution.

2.5 Types of filters

Filters are used in electrical and electronic systems to remove or reduce unwanted signals, such as harmonics in power systems or noise in communication systems. There are different types of filters according to their response characteristics. Some of them are:

2.5.1 Passive Filter

They consist solely of passive components: resistors (R), inductors (L), and capacitors (C). They are simple, cost-effective, and reliable, but have fixed tuning and limited adaptability. Single-tuned filters are designed for a specific harmonic frequency. A High-Pass Filter allows higher frequencies while blocking lower ones. A Low-Pass Filter allows lower frequencies while blocking higher ones. A band-pass filter allows a specific range of frequencies to pass through while attenuating frequencies outside this range.

2.5.2 Active Filter

The APFs compensate for unwanted signals in the system by using power electronics and control algorithms. They generate harmonic components and inject them to cancel load current harmonics. They can also compensate for reactive power and negative sequence currents [8]. Shunt APFs act like current sources, injecting a compensating current I_C, which is 180° out of phase with regard to the load current I_L, to produce a sinusoidal source current at the point of common coupling. The power circuit consists of a voltage source inverter VSI controlled via pulse-width modulation PWM and a DC-link capacitor for storing energy and regulating the voltage [9].

Series APFs inject a series voltage to cancel voltage harmonics, and hybrid active-passive filters use passive filters for the predominant harmonics along with active filters that cancel the additional harmonics, enhancing performance at reduced costs 8. Passive filters have several drawbacks: they are bulky, resonate, and are unstable.

Hence, low-pass and high-pass filters can be used for selective frequency compensation. The APF controller tracks continuously the value of I_L to develop the current I_C in real time, shaping the compensating waveform so that effective harmonic mitigation with THD less than 5% is

maintained [7]. The APF operation can be represented mathematically with I_C and I_L as follows, where the next equations define the relationship between the compensating current, load current, and reference waveform I_s:

$$I_s = I_L - I_C \tag{2.2}$$

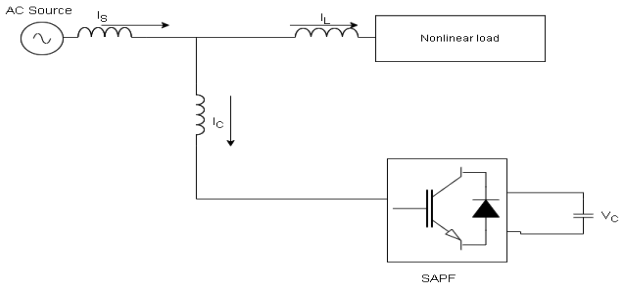

Figure 2. 2 Circuit diagram of shunt active power filter

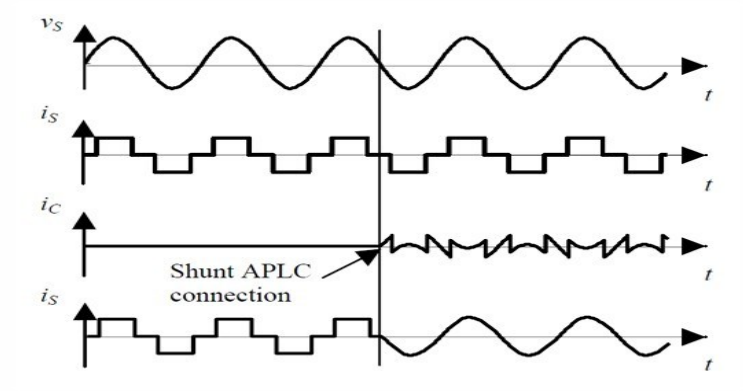

Figure 2. 3 Waveform of source current after connecting filter

The behaviour and effectiveness of the APF shunt in harmonic reduction depend on how current harmonics and reactive power are sensed, along with the compensation control algorithm designed that determines the filter's capability for correct distortion compensation [10]. As a basic theory for controlling the compensation current, the P-Q theory of instantaneous reactive power was widely used, first introduced by Akagi et al. in 1983 [11].

Various techniques have been suggested for extracting harmonic and fundamental components, determining reference compensation currents, and controlling the DC-link voltage [10]. In [12], modified IRPT theory was used to govern the reference compensating current at the point of

common coupling and has shown that an APF installed at the feeder end can effectively limit harmonic propagation and handle both dynamic and steady-state load conditions.

III. Reference Frame Theory:

In the abc-frame, the three axes are 120° apart to represent three-phase voltages and currents, which follow sinusoidal waveforms. The αβ-frame reduces the system to two axes—α (aligned with the a-phase) and β (orthogonal to α)—simplifying control by reducing the number of control loops while keeping sinusoidal voltage and current components.

In balanced systems, the 0 component in the αβ0-frame is zero, while in unbalanced systems with negative and zero sequence components, the 0 component becomes non-zero. The Clarke transform is used to convert abc signals to the αβ-frame, providing a simpler, two-dimensional representation that is suitable for real-time digital control on DSPs and FPGAs. Since the αβ-frame is stationary, it is particularly useful for THD mitigation in grid-tied, stationary systems without requiring a rotating reference frame.

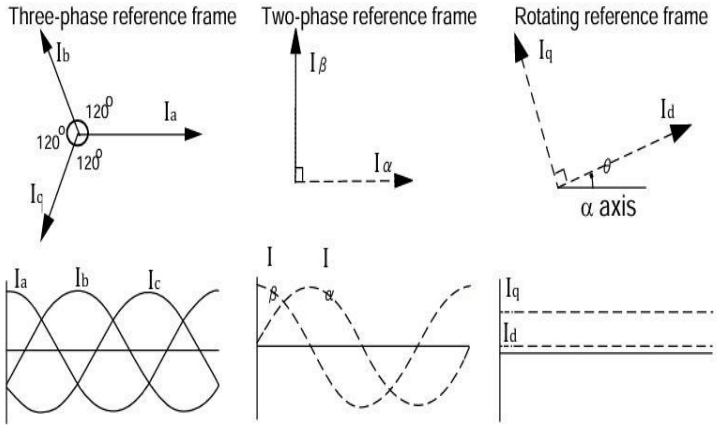

Figure 2. 4 Currents in different reference frame

2.5.3 Harmonic Extraction:

The effectiveness of harmonic extraction and estimation determines the effectiveness of SAPF. An SAPF uses a time-domain or frequency-domain approach to determine the reference current. A time-domain approach is simpler, more computationally lightweight, and hence faster for

controllers. On the other hand, the frequency-domain approach provides much higher precision due to spectral analysis [6].

The PQ theory works in the time domain and is developed under MATLAB/Simulink. It converts the stationary abc-frame to 0-α-β coordinates through Clarke transformation, thus turning a three-phase quantity into two-phase stationary frames representing the voltage and current by two orthogonal vectors. This decoupled representation simplifies real-time analysis and control of power components, facilitating precise harmonic compensation. The representation of the Clark transformation is illustrated in the phasor diagram below:

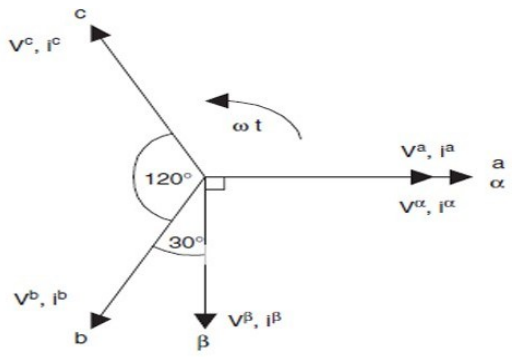

Figure 2. 5 Reference currents in single phasor diagram

The conversion of source voltage and source current into 0-α-β components from abc components is as shown in the following expressions (2.3) and (2.4).

$$\begin{bmatrix} v_0 \\ v_\alpha \\ v_\beta \end{bmatrix} = \begin{bmatrix} \frac{1}{\sqrt{3}} & \frac{1}{\sqrt{3}} & \frac{1}{\sqrt{3}} \\ 1 & -\frac{1}{2} & -\frac{1}{2} \\ 0 & \frac{\sqrt{3}}{2} & -\frac{\sqrt{3}}{2} \end{bmatrix} \begin{bmatrix} v_a \\ v_b \\ v_c \end{bmatrix} \tag{2.3}$$

$$\begin{bmatrix} i_0 \\ i_\alpha \\ i_\beta \end{bmatrix} = \begin{bmatrix} \frac{1}{\sqrt{3}} & \frac{1}{\sqrt{3}} & \frac{1}{\sqrt{3}} \\ 1 & -\frac{1}{2} & -\frac{1}{2} \\ 0 & \frac{\sqrt{3}}{2} & -\frac{\sqrt{3}}{2} \end{bmatrix} \begin{bmatrix} i_a \\ i_b \\ i_c \end{bmatrix} \tag{2.4}$$

In the a-b-c coordinate system, the three-phase voltages are represented as v_a, v_b, and v_c, while the corresponding three-phase currents are denoted as i_a, i_b, and i_c. In the 0-α-β coordinate

system, the voltages are indicated by v_0, vα, and vβ, and the currents are represented as i_0, iα, and iβ.

Total complex power is the sum of active power (p) and reactive power (q), which can be calculated using the following equation (2.5):

$S = p + jq = \boldsymbol{v}_{\alpha\beta}\boldsymbol{i}^{*}_{\alpha\beta}$

$$S = (\boldsymbol{v}_{\alpha} - j\boldsymbol{v}_{\beta})\,(\boldsymbol{i}^{*}_{\alpha} + j\boldsymbol{i}^{*}_{\beta}) = (\boldsymbol{v}_{\alpha} + \boldsymbol{v}_{\beta}\boldsymbol{i}_{\beta}) + j\,(\boldsymbol{v}_{\alpha}\boldsymbol{i}_{\beta} - \boldsymbol{v}_{\beta}\boldsymbol{i}_{\alpha}) \quad (2.5)$$

Where, S represents the complex power, p is given by active power, q denotes the reactive power, and * characterizes the complex conjugate.

Hence, the instantaneous active and reactive power components in the α-β reference frame can be expressed in matrix form as follows:

$$\begin{bmatrix} p \\ q \end{bmatrix} = \begin{bmatrix} v_{\alpha} & v_{B} \\ -v_{B} & v_{a} \end{bmatrix} \begin{bmatrix} i_{\alpha} \\ i_{\beta} \end{bmatrix} \quad (2.6)$$

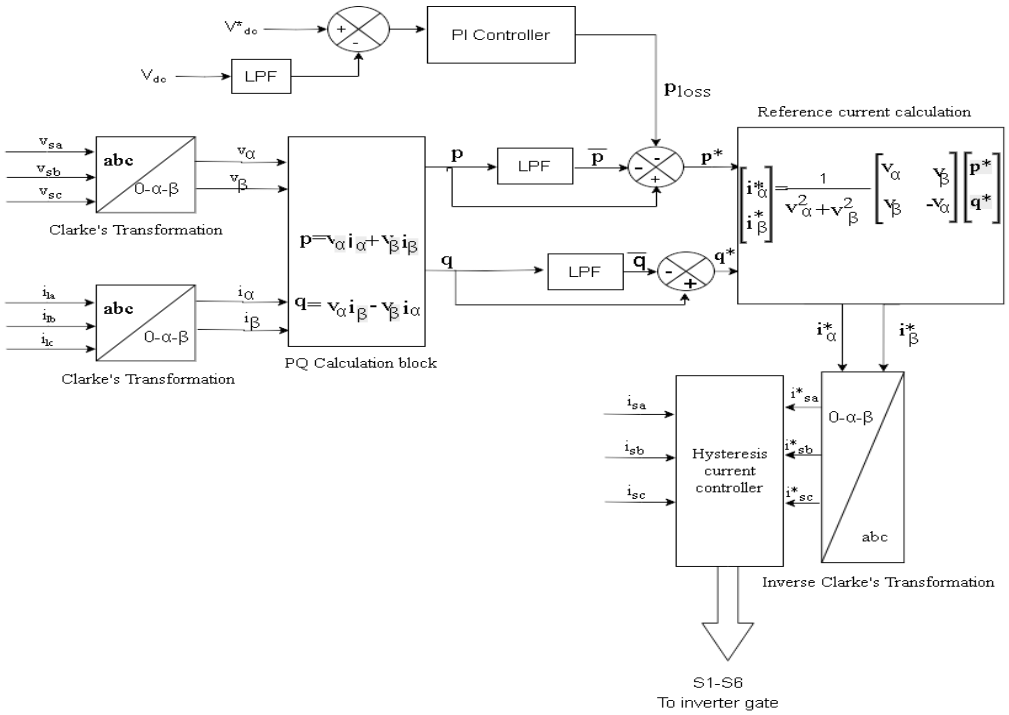

Figure 2. 6 Instantaneous Reactive Power Theory Control Algorithm

In the case of nonlinear loads, instantaneous active and reactive powers are divided into DC and AC parts. The DC part ($\bar{P}$) of the instantaneous active power represents the power delivered

from the source to the load, corresponding to the fundamental voltage and current components. The AC component indicates the energy exchanged between source and load (p^*). The DC component, representing the power the three-phase AC source must supply [9], is extracted by a higher-order low-pass filter. The IRPT-based control schematic is shown in Figure 2.6, which utilizes the DC and AC components for harmonic compensation and real-time control of the shunt active power filter.

Concerning about the instantaneous reactive power component (Q), and q*, shows the fundamental and harmonic component respectively, that is responsible for the flow of energy between the load phases. The instantaneous current of α and β axis are given in equation below [13]:

α – axis instantaneous active current:

$$i_{\alpha}^{p} = \frac{v_{a \cdot P}}{v_{\alpha}^{2}+v_{\beta}^{2}} \quad (2.7)$$

α – axis instantaneous reactive current:

$$i_{\alpha}^{q} = \frac{-v_{\beta \cdot q}}{v_{\alpha}^{2}+v_{\beta}^{2}} \quad (2.8)$$

β – axis instantaneous active current:

$$i_{\beta}^{p} = \frac{v_{\beta \cdot P}}{v_{\alpha}^{2}+v_{\beta}^{2}} \quad (2.9)$$

β – axis instantaneous reactive current:

$$i_{\beta}^{q} = \frac{v_{\beta \cdot q}}{v_{\alpha}^{2}+v_{\beta}^{2}} \quad (2.10)$$

Active and Reactive components

$$p = \bar{p} + p^* \quad (2.11)$$

$$q = \bar{q} + q^* \quad (2.12)$$

The AC component (p*) of the active power and the total reactive power (q) are mandatory for the generation of harmonic reference currents. To compensate for the switching losses in the Voltage Source Inverter (VSI) and to maintain the DC-link voltage at the desired level, the SAPF

needs a small amount of real power ($\bar{p}_{loss}$) from the three-phase AC source or an external power supply. Thus, the AC component (p*) of the active power can be computed by the given equation in (2.13):

AC Component of Active Power for Harmonic Compensation

$$p^* = p - \bar{p} + \bar{p}_{loss} \tag{2.13}$$

Harmonic Reference Current Generation

$$\begin{bmatrix} i_\alpha^* \\ i_\beta^* \end{bmatrix} = \frac{1}{v_\alpha^2 + v_\beta^2} \begin{bmatrix} v_\alpha & -v_B \\ v_B & v_a \end{bmatrix} \begin{bmatrix} p^* \\ q^* \end{bmatrix} \tag{2.14}$$

Phase-a current reference:

$$i_a^* = i_\alpha^* \tag{2.15}$$

Consequently, the compensating reference currents are first determined within the α-β coordinate system and then converted back to the a-b-c coordinate system through the application of the inverse Clarke transformation, as shown in the earlier expression. This procedure facilitates the application of reference currents in the three-phase system, thereby enabling efficient harmonic compensation.

2.5.4 Current Control Technique:

In establishing proper criteria, different control strategies can be compared, and realistic test scenarios selected on which their performance can be evaluated [14]. In the design of an SAPF current control system, different strategies generate control pulses to determine the switching pattern of the inverter. Among these, the hysteresis band current control method is widely used due to its simplicity, rapid dynamic response, high accuracy, and robust stability [15], [16].

The basic aim of the controller is that the load current must track the reference signal within a hysteresis band by producing appropriate switching signals for the VSI. Load currents are sensed and compared with reference values through three hysteresis comparators whose outputs determine the inverter switching states [17]. However, the drawback of this method is that the switching frequency varies in each fundamental cycle, affecting the performance of inverter. There are a number of methods proposed to dampen or reduce these variations.

Based on the hysteresis band configuration, hysteresis current controllers can be classified into fixed-band and sinusoidal-band type. In a sinusoidal-band controller, the hysteresis band varies sinusoidally over a fundamental period as shown in Figure 2.7 whereas the fixed-band controller maintains a constant band, as shown in Figure 2.8 [15].

In the fixed-band approach, the hysteresis band remains constant throughout the fundamental period. The mathematical model for this fixed-band scheme is expressed as follows:

$I_{ref} = I_{max}$ sinwt (2.16)

$I_{up} = I_{ref} + H$ (2.17)

$I_{low} = I_{ref} - H$ (2.18)

In the above expressions I_{up} refers to the upper band, I_{low} is defined as the lower band, In the fixed-band scheme, H represents the hysteresis band limit. Referring to Figure 2.8, when $i_a > i_{up}$, the signal to the controller is 0, indicating that the inverter output voltage switches to negative to reduce the line current. Conversely, when $i_a < i_{low}$, the signal is 1, causing the inverter output voltage to switch to positive to increase the line current.

In contrast, the sinusoidal-band scheme involves a hysteresis band that varies sinusoidally over the fundamental period [15]. Mathematical model of this scheme is given by the following equations:

$I_{ref} = I_{max}$ sinwt (2.19)

$I_{up} = (I_{max} + H)$ sinwt (2.20)

$I_{low} = (I_{max} - H)$ sinwt (2.21)

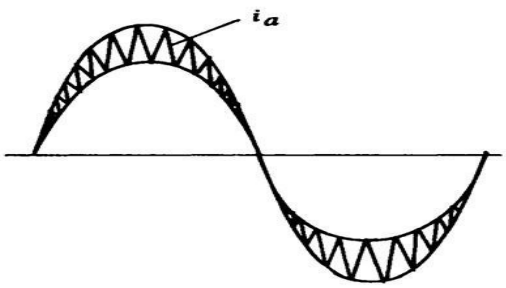

Figure 2. 7 Hysteresis current controller waveform in sinusoidal frame

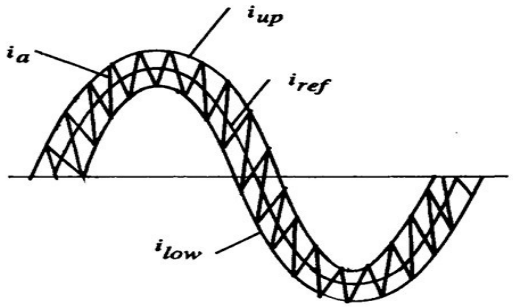

Figure 2. 8 Hysteresis current band in fixed frame

The actual current (i_{sa}, i_{sb}, i_{sc}) and the reference current (i_a*, i_b*, i_c*) are compared to generate an error signal, which is then fed into the inverter. This causes the VSI switches to continuously turn on and off in order to keep the actual current within the hysteresis band. When the current error exceeds the upper threshold of the hysteresis band, the inverter adjusts accordingly, the output of theVoltage Source Inverter (VSI) is turned off, and conversely, it is turned on when the error drops below the lower limit. Generally, the DC voltage attains its peak value when there is a requirement to raise output current, and drops to its lowest value when a reduction in current is necessary [9].

2.5.5 Proportional Integral (PI) Controller:

A. Proportional (P) controller: In a controller utilizing proportional control action, the relationship between the controller output m (manipulated variable) and the error signal e(deviation) is linear [18] .

Mathematically,

$m(t) = K_p\, e(t)$

After Laplace transformation,

$M(s) = K_p\, E(s)$ (2.22)

or, $K_p = M(s)/E(s)$ (2.23)

Where K_p is recognized as proportional gain or proportional sensitivity.

B. Integral Controller: In a controller with integral control action, the controller output changes at a rate proportional to the integral of the actuating error signal e(t). Mathematically,

$\frac{dm(t)}{dt}$ =K_i e(t) (2.24)

where, K_i is constant.

M(t) = $K_i\int$e(t) +m (0) (2.25)

After Laplace transform,

s M(s) = K_i E(s) (2.26)

$\frac{M(s)}{E(s)} = \frac{k_i}{s}$ (2.27)

Above equation (2.26) [18] is the transfer function of integral controller.

C. PI controller: A Proportional-Integral (PI) Controller is a widely used control algorithm in power electronics, industrial automation, and motor drives. It is a type of closed-loop controller that improves system performance by adjusting the control input based on both the present and past errors [18].

The control output m(t) of a PI controller is given by:

m(t) = K_pe(t)+ K_p $K_i\int$e(t)dt (2.28)

or, m(t) = K_p e(t) + $K_p\left(\frac{1}{Ti}\right)\int$ e(t) dt (2.29)

Laplace transform,

M(s) = K_p E(s) + $\frac{k_P}{sT_i}$E(s) (2.30)

M(s) = E(s) [1+$\frac{1}{sT_i}$] K_p (2.31)

$\frac{M(s)}{E(s)}$= K_p [1 + $\frac{k_P}{sT_i}$] (2.32)

where,

K_p = Proportional gain (affects response speed and stability)

K_i = Integral gain (eliminates steady-state error)

e(t)= Error signal

A critical role of the SAPF is to keep the DC-link voltage of the VSI constant for efficient harmonic compensation. A capacitor that stores energy is normally connected in the DC side of the VSI. Ideally, the voltage across it is constant, and no real power is exchanged. In real applications, due to the switching of the VSI, a small amount of real power is drawn by the VSI, and a PI controller is used to keep Vdc at its reference value, eliminating steady-state errors and allowing precise harmonic current compensation [19]. The control scheme for DC-link regulation is shown in Figure 2.9.

Research works have focused on harmonics injected by EV chargers and different compensation methods. Estimation-based SAPF sizing, active compensation, and other advanced filtering methods such as Kalman filter and sliding mode controller are some of the proposed methods. In fact, for higher EV penetrations, the control of SAPF is optimized by using some intelligent algorithms to further improve the harmonic suppression capability of the SAPF. One new design of a PI controller optimized by the Criminal Search Optimization Algorithm (CSOA) was tested in MATLAB/Simulink and also in real-time using an OPAL-RT simulator. Its performance showed improvements compared to PSO, WOA, ACO, and BCO methods.

Harmonic-parameter-based analytical models have been proposed to estimate the capacity of SAPF, validated through simulations and experimental data from EV charging [20]. These works study three-phase uncontrolled rectifier chargers operating under both continuous and discontinuous conduction modes. They estimate parameters such as DC voltage, filter inductance, and load resistance using measured AC waveforms. The DC and AC charging pile models help evaluate harmonics generated in the process of rectification and power conversion and also the electromagnetic interference emissions from charging stations [21].

Comprehensive researches on smart EV charging have pointed out the variability of harmonic emissions with model, battery capacity, and onboard chargers [22]. For example, most EVs charged with lower current setpoints tend to have higher harmonic distortions (THDI). For example, Peugeot e2008 has 11–26% THDI; Tesla Model Y Long Range and Renault Zoe had similar harmonic magnitudes. These results emphasize the necessity of harmonics-aware smart charging with probabilistic modeling in order to minimize harmonic impact on the grid.

The limited experimental data published demonstrate that harmonic distortion varies significantly among EV models and can exceed IEC limits even when PFC is implemented [23]. Superposition of harmonics with other nonlinear loads, such as appliances, further complicates the distortion profile in residential and office environments. Low-order harmonics are susceptible to voltage waveform shape variations, while supraharmonic emissions from PFC stages and downstream converters generally show up around the switching frequency and its harmonics, with broadband components below 10 kHz [23]. These findings again strongly underscore the need for realistic grid conditions in the measurement of harmonics.

2.5.6 IEEE Standard for Harmonics:

To limit the harmonic currents into the power system, IEEE Standards Association has established guidelines and limitations regarding harmonic standards (IEEE Std 519-1992 [24]), which was further refined in 2014 (IEEE Std 519–2014). From this standard the voltage THD shall not exceed 5% for 11kV voltage level and current THD shall not exceed 5% for ratio of short circuit current to full load line current less than twenty [24]. This work explores various sources of harmonics, including VAR compensators, cyclo-converters, switch-mode power supplies, pulse width modulated drives, inverters used in distributed generation, and waveform distortion caused by harmonics. It also analyses distortions in low-voltage distribution feeders, industrial networks, and transmission systems. Furthermore, it addresses the impact of harmonic distortion on the performance of several devices or loads such as motors, generators, transformers, power cables, capacitors, and electronic equipment is discussed.

The nonlinear current drawn by the EV charger creates a harmonic loss in the line. The harmonic line loss depends on THD and the total line losses. As discussed in [25], from equation 5 and 17, copper losses are proportional to I_{rms}^2R and RMS current in presence of harmonics is

$$I_{rms}^2 = I_1^2 \times (1 + THD^2) \tag{2.32}$$

Therefore,

$$P_{harm} = P_{fund} \times THD^2 \tag{2.33}$$

$$P_{harm} = (P_{total} - P_{harm}) \times THD^2$$

$$P_{harm} \times THD^2 + P_{harm} = P_{total} \times THD^2$$

$$P_{harm} \times (1+THD^2) = P_{total} \times THD^2$$

$$P_{harm} = \frac{Ptotal}{1+THD^2} \times THD^2 \quad (2.34)$$

Also, [26] discusses the base THD for 11kV distribution feeder with residential nonlinear loads, small VFDs, SMPS, etc. is between 1 % to 3%. Unlike mitigation-focused studies, this work aims to determine the extent to which additional EV charging load can be integrated into the Sanepa feeder without violating the permissible 5% THD limit as defined by IEEE standards.

CHAPTER 3: METHODOLOGY

This chapter describes the methodology adopted to study the impact of an electric vehicle (EV) charging station on the Sanepa distribution feeder in Kathmandu Valley. The study focuses on the harmonic analysis of the feeder under EV charging conditions and determining the maximum number of EV chargers that can be integrated without exceeding the IEEE 519 THD limit of 5%.

3.1 Approach

Initially, a literature review was carried out to understand the concepts of harmonic analysis, the impact of harmonics on low-voltage distribution networks, the importance of harmonic assessment, and the relevant standards for power quality. The data required for the research was then collected from the NEA Baneshwor office, Thapathali Switching Station, Teku Substation, and from several EV charging stations along the Sanepa feeder, including Sajha Yatayat charging station, NEA charging station, MG charging station, Hyundai charging station, and BYD charging station. The collected data, such as transformer specifications, feeder line length, existing load profiles, and charger characteristics, was used in developing an accurate simulation model of the Sanepa feeder in MATLAB/Simulink.

The model includes the distribution grid, feeder, and EV charging stations, and simulations were executed to analyze THD at different points of the feeder. THD results were compared with the IEEE 519 standard (≤5%) to ensure compliance. Further simulations were performed by incrementally adding additional EV chargers at different buses of the feeder to find the maximum number of EVs that can be integrated without exceeding the permissible limit of THD. Finally, the entire process right from data collection, the simulation setup, and THD analysis was documented in detail so as to present a clear assessment regarding the impact of EV charging on feeder power quality.

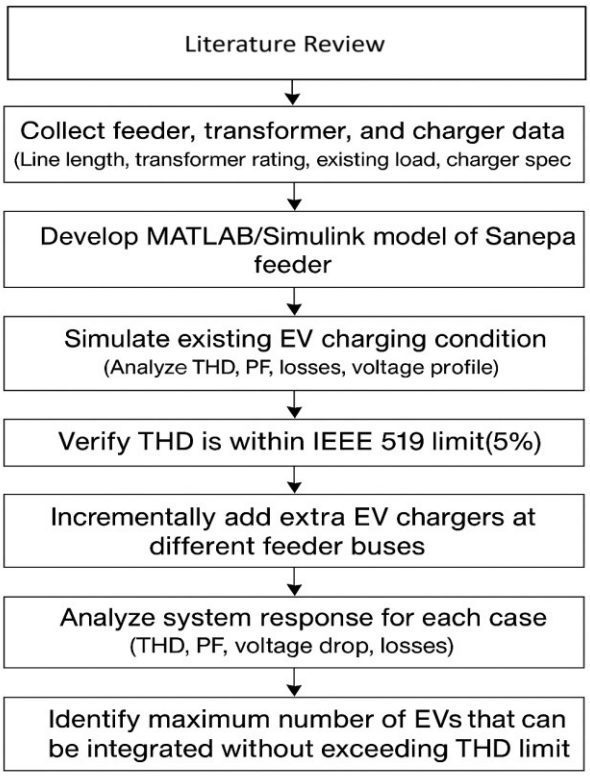

Figure 3. 1 Flowchart of the approached methodology

3.2 Data Collection

3.2.1 Existing Sanepa feeder

The EV charging stations are to be provided with a 3-phase, 400V, 50Hz AC supply through the distribution transformers connected an 11kV feeder line as per the NEA specifications. This work conducts the study of total harmonic distortion on the Sanepa distribution feeder of Kathmandu valley due to an electric vehicle charging station. The feeder is supplied by Thapathali Switching Station. This feeder consists of around 20 transformers, and the feeder length is 9.6km. This 11kV system consists of commercial as well as residential loads.

A 45 MVA, 132/11 kV transformer with 11.62% impedance was obtained from the Thapathali Switching and Teku Substation. Figure. 3.2 shows a GIS map view and figure 3.3 shows the single line diagram:

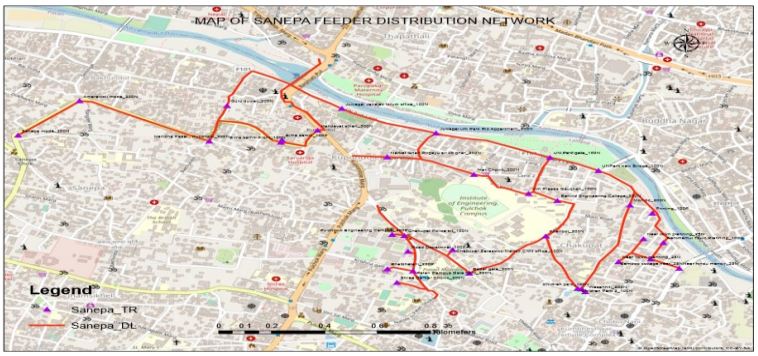

Figure 3. 2 GIS map view of Sanepa Feeder

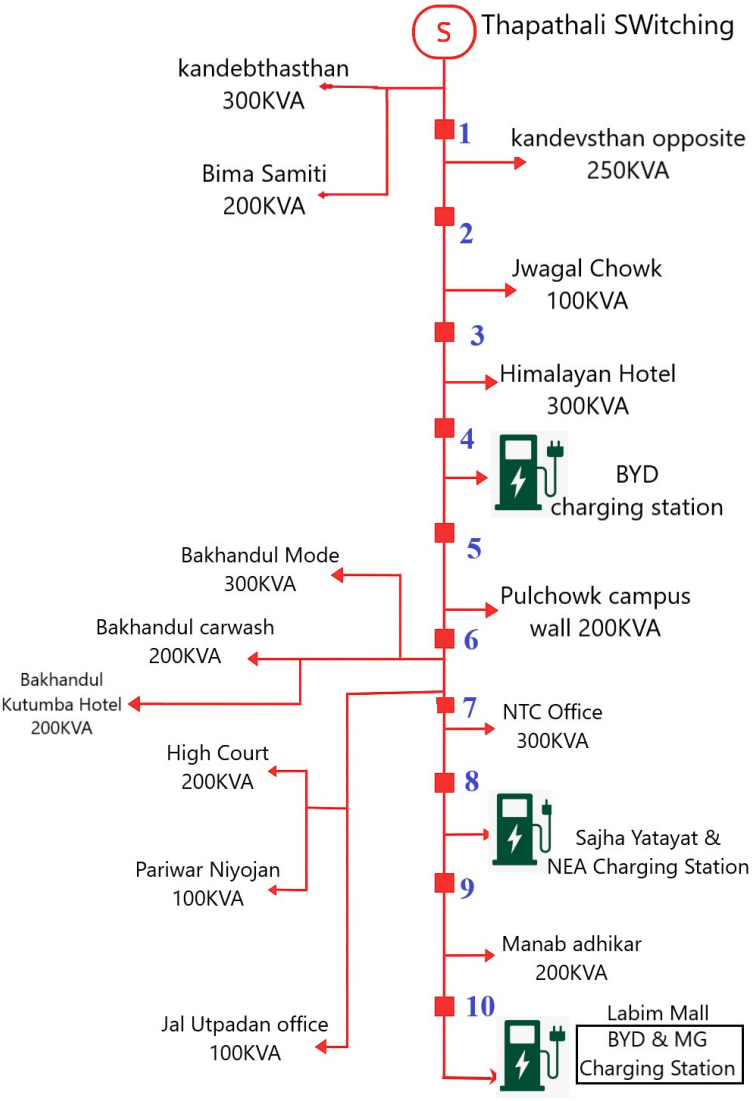

Figure 3. 3 SLD of Sanepa feeder

3.2.2 Existing EV chargers' data

Table 3. 1 EV charger specifications

Charging stations	Transformer rating Tx(kVA)	Numbers of EV chargers	Current capacity CC(A)	Power P(KW)	Total power (KW)
Sajha Yatayat	500	5	315	90	450
	200	2	315	90	180
	200	2	315	90	180
	200	2	315	90	180
NEA charging station	200	1	315	120	120
	200	1	315	120	120
	200	1	315	120	120
mg charging station	100	1	32	7	7
		1	32	7	7
Hyundai charging station	100	1	32	7.3	7.3
Byd charging station	200	1	120	40	40
		1	120	40	40

Table 3.1 summarizes the EV charger specifications across different stations. Sajha Yatayat has 5 chargers on a 500 kVA transformer and multiple 200 kVA transformers totaling 990 kW. NEA has three 200 kVA transformers supplying 120 kW chargers. Mg and Hyundai stations use 100 kVA transformers for small chargers (7–7.3 kW), while Byd has two 200 kVA transformers supplying 40 kW chargers each.

3.3 System Modelling

The feeder is modelled in the MATLAB/Simulink environment. Initially, the model was developed to analyze the system behavior before the integration of EV chargers. Then EV charger is integrated into the system to evaluate its impact on the performance of the feeder.

3.3.1 Thapathali Switching Source Data

Table 3. 2 Thapathali switching source data

Parameter Details	
System Frequency	50Hz
Transformer voltage level	11/0.4kV
Size	45 MVA
Percentage impedance	11.62%
Short Circuit MVA	400 MVA
X/R ratio	3
Short-circuit current (I_{sc})	≈ 21 kA
Rated transformer current (I_L)	≈ 2.36 kA
I_{sc}/I_L ratio	≈ 8.9

Table 3.2 presents the source transformer data obtained from the Thapathali Switching Substation. The transformer has a capacity of 45 MVA with a voltage level of 11/0.4 kV and operates at a system frequency of 50 Hz. It has a percentage impedance of 11.62%, corresponding to a short-circuit level of approximately 400 MVA, and an X/R ratio of 3. The short-circuit MVA is calculated using the following mathematical relation:

Mathematical aids for short-circuit MVA calculation:

$$\text{Short-circuit MVA} = \frac{\text{Transformer Rating (MVA)}}{\text{Percentage Impedance}} \times 100$$

Substitute values:

$$\text{Short-circuit MVA} = \frac{45}{11.62} \times 100 = 387.26 \text{ MVA} \approx 400 \text{ MVA}$$

3.3.2 Feeder Transformer Data

Table 3. 3 Feeder transformer internal parameters

S (kVA)	Zpu	Rtotal_pu	Xtotal_pu	R1=R2 (pu)	L1=L2 (pu)
100	0.04	0.00784	0.0392	0.00392	0.0196
200	0.04	0.00784	0.0392	0.00392	0.0196
250	0.045	0.00882	0.0441	0.00441	0.0221
300	0.045	0.00882	0.0441	0.00441	0.0221
500	0.05	0.0098	0.049	0.0049	0.0245

Table 3.3 shows the internal per-unit parameters of the feeder transformers, including impedance, resistance, and reactance values for different transformer ratings used in the Sanepa Feeder model. A total of 28 transformers is installed across the Sanepa Feeder and associated charging stations. Among them, the majority are 200 kVA units, totaling 13 in number, followed by 8 transformers rated at 100 kVA. There are 5 transformers of 300 kVA capacity, while single units of 250 kVA and 500 kVA are also present. This distribution highlights a predominant use of medium-capacity transformers, particularly in the 100 kVA to 300 kVA range, with one high-capacity 500 kVA.

3.3.3 Line parameters

The distribution lines in the Sanepa feeder are modeled using a short transmission line RL model, which captures the series resistance and inductance along with the shunt capacitance effects for accurate analysis. Both positive and zero sequence parameters are considered to represent normal and unbalanced operating conditions in the network.

Table 3. 4 line parameters

Resistance(ohms/km)	Inductance(H/km)
0.1273	9.34E-04

Table 3.4 lists the line parameters, including resistance, inductance, and capacitance per kilometer for positive and zero sequence, used in the feeder modeling.

3.3.4 Load division on Feeder transformer

Table 3. 5 Load allocation on feeder transformers

Actual TX KVA	70% KVA	pf	KW	KVAR	KW/phase	KVAR/phase
300	210	0.95	199.5	65.57	66.5	21.86
250	175	0.95	166.25	54.67	55.42	18.22
200	140	0.95	133	43.72	44.33	14.57
100	70	0.95	66.5	21.86	22.17	7.29

Table 3.5 presents the load division on Sanepa feeder transformers. For the load analysis, each feeder transformer is assumed to operate at 70% of its rated capacity to reflect typical initial

loading conditions. The power factor is taken as 0.95, representing mostly inductive distribution loads. Using these assumptions, the total active and reactive power for each transformer is calculated and then divided per phase for three-phase modeling. This load division allows accurate simulation of voltage profiles, losses, and other analysis across the network. Smaller transformers carry proportionally lower loads, while larger units handle higher power, ensuring a realistic representation of the feeder operation.

3.4 EV station modelling

A three-phase DC fast charger model for various brand was developed in MATLAB/Simulink to analyze the operational behavior of EV charging systems connected to a medium-voltage distribution feeder.

3.4.1 Model of Ev charger

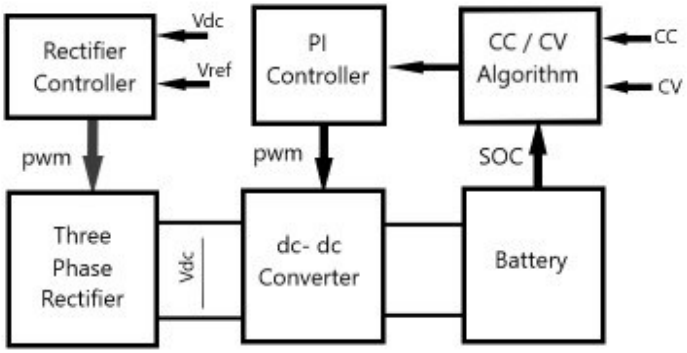

Figure 3. 4 Block diagram of Ev charger

Figure 3.4 shows the block diagram of EV charger modelling. A general charger design has three main stages: a controlled rectifier, a DC–DC converter, and the battery charging control stage under a CC–CV algorithm.

AC input is converted to regulated DC voltage by a three-phase controlled rectifier in the first stage. The output voltage, Vdc, is continuously compared with the reference voltage, Vref, and a closed-loop rectifier controller using a PID algorithm maintains the DC link voltage at the desired level. In the second stage, a buck-type DC–DC converter steps down the regulated DC voltage for charging purposes. The converter's duty ratio is controlled by a PI controller maintaining the desired current or voltage depending on the mode of charging.

The battery charging algorithm is implemented through the use of MATLAB functions that automatically switch between CC and CV modes based on the battery's state of charge. At less than 80% SOC, the system provides constant current in CC mode; after this, it operates in CV mode, wherein a fixed voltage is maintained with a gradual decrease in current. The proposed model of a battery takes into account the internal resistance, capacity, and estimation of SOC, which presents realistic dynamics of battery charging.

By changing CC, CV, and battery parameters, the charger model can be made representative of different EV brands with a particular type of battery specification. An integrated system therefore offers flexibility in control and gives an accurate performance evaluation of the EV charger and its potential impact on the distribution feeder under various operational conditions.

3.4.2 Chargers modelled for analysis

Table 3. 6 Modeled EV Charger Data for Simulation Analysis

SN	Charging stations	Transformer rating Tx(kVA)	NO. of chargers	Current capacity CC(A)	Power rating P(KW)	Total power (KW)
1	Sajha Yatayat	500	5	315	90	450
		200	1	630	180	180
		200	1	630	180	180
		200	2	315	90	180
2	NEA charging station	200	1	315	120	120
		200	1	315	120	120
		200	1	315	120	120
3	mg charging station	100	1	64	14	14
			1	32	7	7
4	Hyundai charging station	100	1	32	7.3	7.3
5	Byd charging station	200	1	120	40	40
			1	120	40	40

Table 3.6 shows the EV chargers modeled for simulation in the Sanepa feeder network. For computational efficiency, multiple individual chargers at a station are aggregated into a single equivalent charger, with total power equal to the sum of the individual units. For example, two 90 kW chargers at Sajha Yatayat are modeled as a single 180 kW charger. Similarly, multiple 7 kW chargers are combined, where applicable. This simplification reduces simulation time in MATLAB, without significantly affecting the results. This modeling approach has a corresponding effect on Total harmonic distortion and power factor were analyzed; the values obtained were shown to be negligible so the contribution from the reduced model also maintains the accuracy of network behaviour.

3.5 Cases studies

In order to analyze the impact of electric vehicle (EV) charging on the Sanepa feeder network, multiple case studies were conducted considering different time frames, load conditions, and EV penetration levels. These studies are divided into existing load scenarios and future expansion scenarios. The analysis considers both "crowded" and "distributed" conditions, where crowded represents locations with additional EVs added to existing charging points, and distributed represents locations farther along the feeder with new EV installations.

3.5.1 Study on existing cases

Table 3. 7 Existing EV Charging Scenarios on Sanepa Feeder

Cases	Time frame	Scenario	BYD	Sajha	NEA	MG	Hyundai	Total Power (kW)	% EV Penetration
1	Morning	Normal	1	2	1	1	1	354.3	24.42
2		Maximum	2	4	2	2	1	701.3	48.33
3	Afternoon	Normal	1	2	1	1	1	354.3	24.42
4		Maximum	2	4	2	2	1	701.3	48.33
5	Evening	Normal	1	5	1	1	1	624.3	43.02
6		Maximum	2	7	2	2	1	971.3	66.93
7	Night	Normal	1	8	2	1	0	1007	69.39
8		Maximum	1	9	3	2	1	1231.3	84.85
9	Full load condition		2	11	3	2	2	1451.3	100

Table 3.7 summarizes the existing EV charging scenarios across different time frames of the day (morning, afternoon, evening, and night). For each scenario, the number of EV chargers at BYD, Sajha Yatayat, NEA, MG, and Hyundai stations is indicated along with the total charging power

(kW) and the percentage of EV penetration relative to the feeder's capacity. Normal scenarios represent typical loading, while maximum scenarios reflect peak EV charging demand. This provides a baseline for understanding how the current EV distribution affects voltage profiles, power factor, and network losses. Figure 3.5 visually represents the total EV load distribution for these existing scenarios.

3.5.2 Load profile

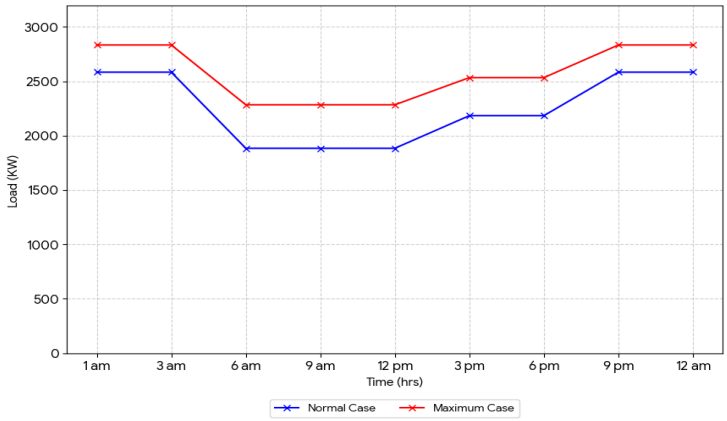

Figure 3. 5 Daily EV load profile

3.5.3 Future expansion Crowded case

For the crowded case, additional EV chargers are assumed at existing charging locations, simulating high-demand conditions. The additional EV charges are assumed to be add at Manab Adhikar and NTC office i.e. node 7 and 9 respectively since these are the only available node for analysing the crowded case and node 5 isn't considered due to college premises nearby.

Table 3. 8 Proposed EV Additions – Future Expansion (Crowded Case)

Node	Position	Wattage	No.	Total Wattage (kW)
7	NTC office	90	4	360
9	Manab Adhikar office	120	2	240
				600

Table 3.8 lists the proposed new EV installations, including node positions, individual charger wattage, number of chargers, and total power per node. The cumulative effect of this added load

helps in assessing feeder performance under high EV penetration. Figure 3.5 illustrates the crowded EV distribution along the feeder.

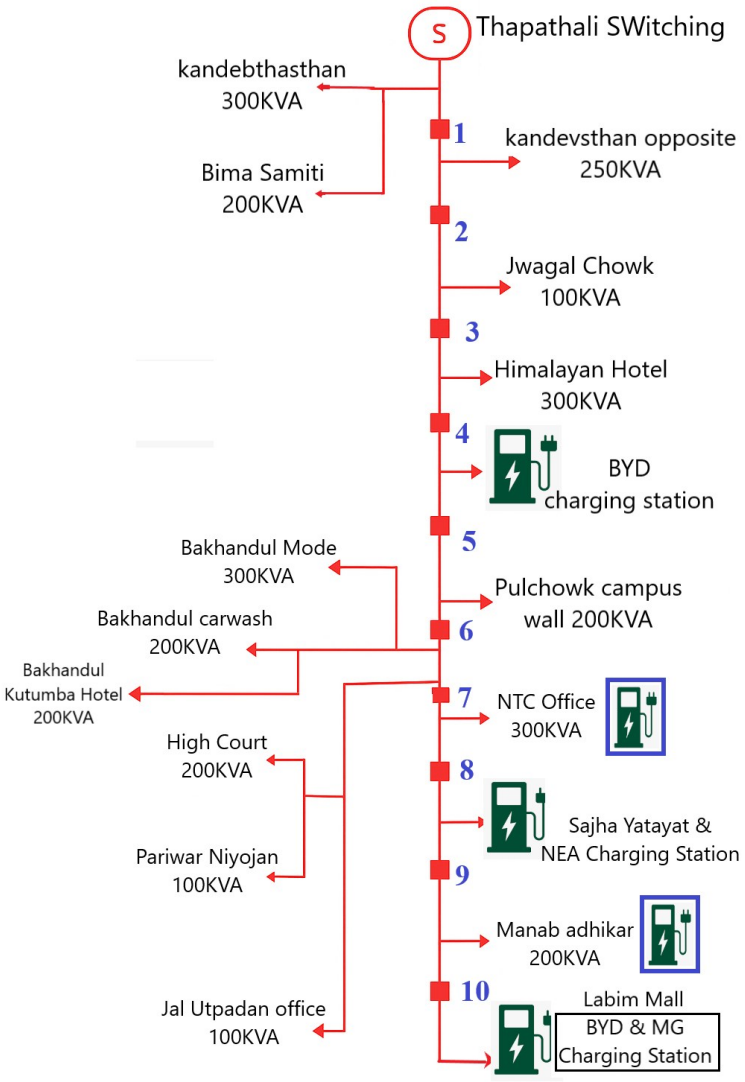

Figure 3. 6 EV Load Distribution – Crowded Scenario on Sanepa Feeder

3.5.4 Future expansion Distributed case

In the distributed case, new EVs are added at nodes farther from the existing charging points to represent a more distributed charging scenario. The additional EV chargers are added to the the Himalayan hotel and Bakhundol kutumba hotel i.e. at node 3 and 12 respectively because there

are enough available spaces in hotel area and users can have easy access to the EV charger while living in the hotel.

Figure 3.6 shows the spatial distribution of EV chargers under the distributed scenario, enabling comparison with crowded conditions and assessment of voltage drop, losses, and harmonics along the feeder.

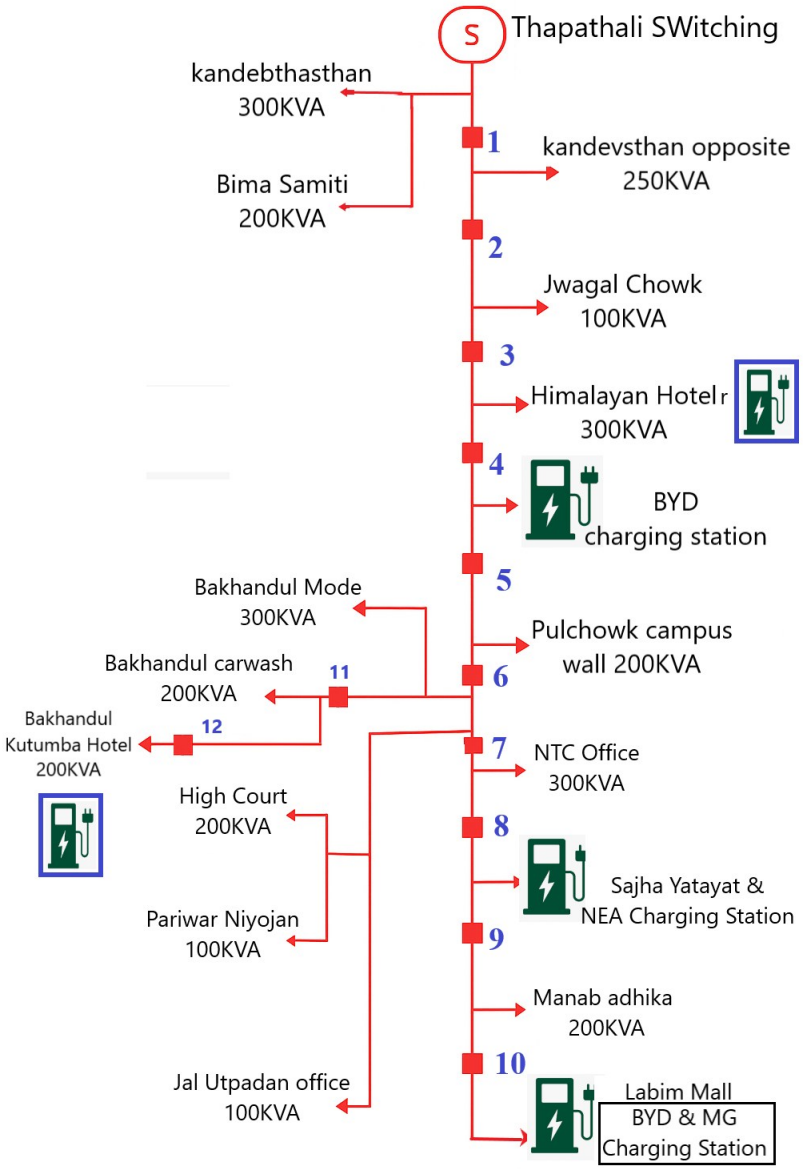

Figure 3. 7 EV Load Distribution – Distributed Scenario on Sanepa Feeder

Table 3. 9 Proposed EV Additions – Future Expansion (Distributed Case)

Node	Position	Wattage	No.	Total Wattage (kW)
3	Himalayan Hotel	120	2	240
12	Bakhundol Kutumba Hotel	120	2	240
		90	4	360
				840

Table 3.9 provides details of these additional EV loads, including node positions, charger ratings, quantity, and total power contribution. The total added load in this scenario is 840 kW, representing moderate EV penetration along the feeder length.

The placement of additional EV chargers, as per the proposed Crowded and Distributed future expansion scenarios, in offices like the NTC office and Manab Adhikar office, and hotels like Himalayan Hotel and Bakhundol Kutumba Hotel, reflects sound real-world planning for high EV penetration. These are chosen primarily because they inherently would offer extra physical space and typically have adequate electrical infrastructure that could easily accommodate new charging stations. Of greater importance, they are common destinations where vehicles are parked for extended periods-during work hours at offices and overnight at hotels-and are thus apt to utilize a range of charging speeds. This positioning is in anticipation of future market demand: as EV ownership rises, hotels will be required to provide charging as an essential guest amenity, and offices will increasingly offer charging facilities to employees as a key benefit, ensuring that the study assesses feeder performance under realistic and diverse high-demand conditions.

CHAPTER 4: RESULTS AND DISCUSSIONS

4.1 Normal Case

The analysis of the feeder under normal conditions is performed to establish a baseline for voltage profiles, power losses, power factor, and total harmonic distortion (THD). The normal case considers typical loading without any additional EV penetration.

Table 4. 1 Feeder Performance under Normal Operating Condition

NODE	PF	THD (phase A)	voltage(pu)
1	0.9368	0	0.9967
2	0.937	0	0.9963
3	0.9372	0	0.996
4	0.9373	0	0.9957
5	0.9375	0	0.9954
6	0.9377	0	0.9951
7	0.9378	0	0.9949
8	0.9381	0	0.9948
9	0.9377	0	0.9948

Branch	power loss(W)
1-2	49.94
2-3	45.28
3-4	33.72
4-5	33.72
5-6	33.73
6-7	25.47
7-8	0.4535
8-9	0.4538

Table 4.1 presents the baseline performance of the Sanepa feeder without EV charging load. The power factor remains steady around 0.937 with negligible THD, and voltage stays close to 1 p.u. across all nodes, indicating a well-balanced and stable operating condition with minimal power losses along the feeder branches. Since residential nonlinear loads such as small VFDs, LED drivers, and household electronics were not included in the model, the background THD appears as 0% in the analysis.

4.2 EV Charger Analysis

Figure 4.1 and Figure 4.2 illustrates the SOC, voltage, current, and power output characteristics of the NEA 120 kW, 315 A charger operating in constant current and constant voltage mode respectively. In CC mode, the initial state of charge is 70% and EV starts charging at a constant current of 315A consuming power of 120KW. In time period of 0.5 sec, the SOC rises from 70% to 70.09% i.e. the state of charge increases by 0.09%. The chargers operate from CC to CV mode when SOC exceeds 80%. In CV mode, the initial state of charger is 81% and EV starts charging at a constant voltage of 370V consuming power of around 9kW.

In CC mode at time period of 0.5 sec, the SOC rises from 70% to 70.09% i.e. the state of charge increases by 0.09% while in CV mode, for the same time period of 0.5 sec, the SOC rises from 81% to 81.0068% i.e. the state of charge increases by 0.0068%. We can clearly observe that the EV charger consumes much more power and charges rapidly in CC mode than in CV mode ensuring the fast charging in CC mode and safe charging in CV mode.

Similarly, the performance waveforms for other EV charges are shown in the Appendix.

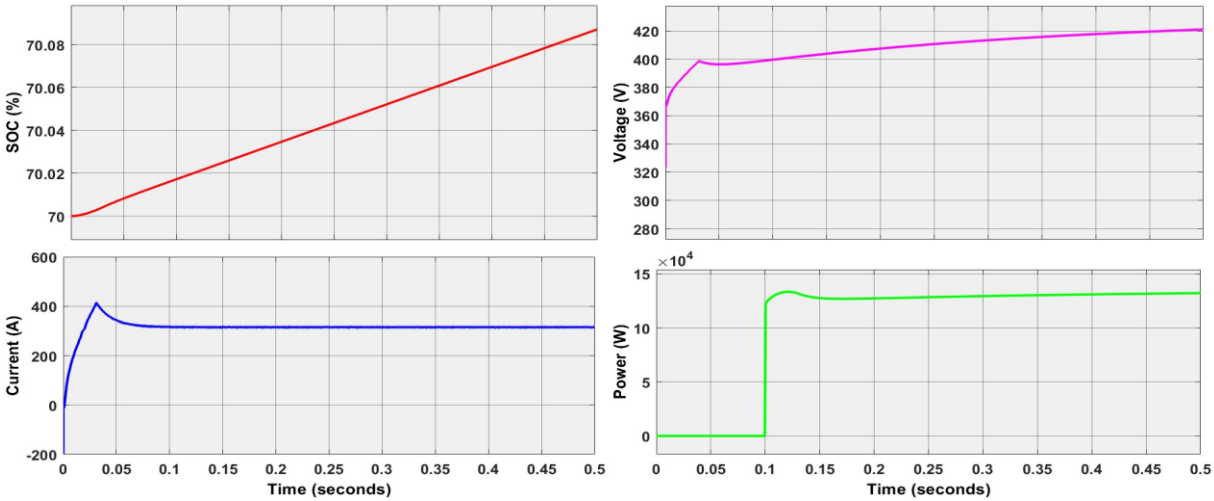

Figure 4. 1 Performance Waveforms of NEA charger in CC mode

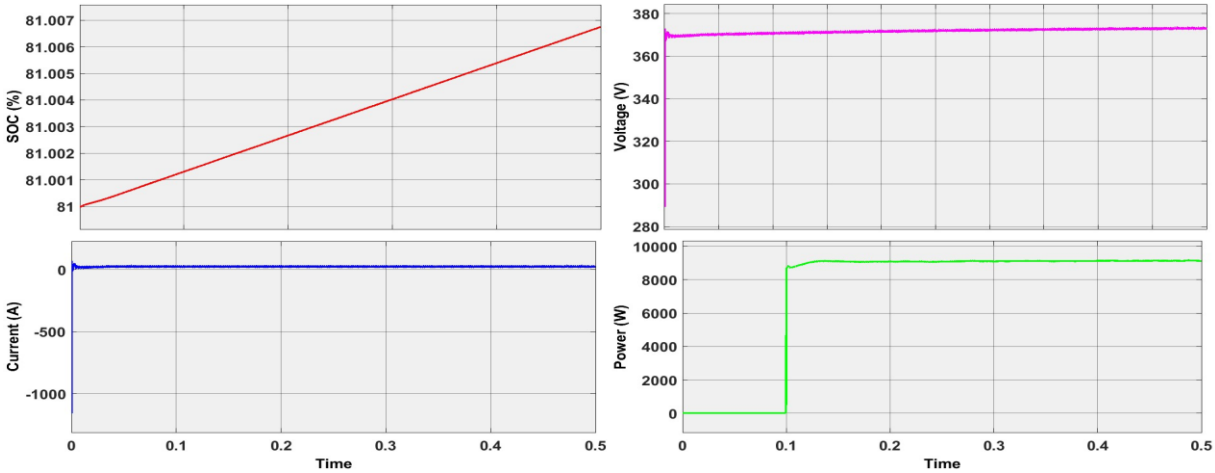

Figure 4. 2 Performance Waveforms of NEA charger in CV mode

4.3 Comparison of 90 kW and 180 kW Chargers

A comparative analysis is performed between individual 90 kW chargers and aggregated 180 kW chargers to assess the impact on voltage profile, power loss, power factor, and THD.

Table 4. 2 Impact Comparison of Aggregated vs. Individual EV Chargers

Node	THD			pf			Voltage (pu)		
	180 KW	90*2 KW	% Error	180 KW	90*2 KW	% Error	180 KW	90*2 KW	% Error
1	0.6	0.6	0	0.9274	0.9223	0.55	0.995	0.9952	0.02
2	0.73	0.73	0	0.9272	0.9216	0.6	0.9944	0.9947	0.03
3	0.87	0.87	0	0.9273	0.9215	0.63	0.9939	0.9941	0.02
4	1.01	1.01	0	0.9268	0.9203	0.7	0.9933	0.9936	0.03
5	1.15	1.15	0	0.9272	0.9207	0.7	0.9928	0.9931	0.03
6	1.29	1.29	0	0.927	0.9198	0.78	0.9923	0.9926	0.03
7	1.43	1.43	0	0.9218	0.9091	1.38	0.9918	0.9922	0.04
8	1.58	1.58	0	0.9188	0.9026	1.76	0.9916	0.9919	0.03
9	1.58	1.58	0	0.9366	0.9365	0.01	0.9915	0.9919	0.04

Table 4.2 compares network parameters—voltage, power factor (PF), and total harmonic distortion (THD)—for aggregated 180 kW chargers and individual 90 kW chargers. For modeling efficiency, multiple chargers at a station (e.g., two 90 kW chargers at Sajha Yatayat) are combined into a single equivalent unit. The results confirm the negligible THD differences, slight PF variations of up to 1.76%, and minimal voltage deviations of up to 0.04 pu. This means that the aggregation has been correctly done and represents the real scenario while reducing the simulation burden with MATLAB significantly. This approach will ensure a realistic yet computationally efficient analysis of the Sanepa feeder network.

4.4 Nine Case Scenarios

The nine cases discussed in Section 3.5.1 are analyzed in detail focusing on Case 8 and Case 9 due to high EV penetration levels. The analysis includes voltage profiles along nodes, power loss along branches, power factor along nodes, and THD along nodes.

Table 4. 3 Case 1 – Morning Normal EV Scenario

CASE 1						
NODE	PF	THD (phase A)	voltage(pu)		Branch	power loss(W)
1	0.8713	0.97	0.991		1-2	458
2	0.8691	1.2	0.9897		2-3	434
3	0.8688	1.42	0.9885		3-4	387
4	0.8655	1.65	0.9873		4-5	302
5	0.8732	1.83	0.9863		5-6	296
6	0.8708	2.01	0.9853		6-7	271
7	0.8492	2.2	0.9843		7-8	146
8	0.8401	2.41	0.9836		8-9	35.6
9	0.6501	2.47	0.9833		9-10	30.7
10	0.6011	2.55	0.983			

Table 4. 4 Case 2 – Morning Maximum EV Scenario

CASE 2						
NODE	PF	THD (phase A)	voltage(pu)		Branch	power loss(W)
1	0.8824	1.18	0.9878		1-2	810
2	0.882	1.45	0.986		2-3	778
3	0.8826	1.72	0.9842		3-4	714
4	0.8816	2	0.9825		4-5	587
5	0.8861	2.24	0.981		5-6	580
6	0.8856	2.49	0.9796		6-7	546
7	0.8769	2.75	0.9781		7-8	359
8	0.8741	3.04	0.977		8-9	27
9	0.7136	3.04	0.9766		9-10	22.7
10	0.6429	3.06	0.9764			

Table 4.3 shows voltage, PF, THD, and branch losses under a normal morning load. THD is low (<2.5%) and voltage remains close to 0.983–0.991 pu. Power losses are moderate along the feeder. This scenario represents minimal EV penetration (24.42%).

Table 4.4 shows voltage slightly lower than Case 1 due to increased load. THD rises to ~3%, and branch losses increase significantly. PF remains fairly high. This scenario shows peak morning EV charging (48.33%), highlighting early network stress.

Table 4. 5 Case 3 – Afternoon Normal EV Scenario

CASE 3						
NODE	PF	THD (phase A)	voltage(pu)		Branch	power loss(W)
1	0.8713	0.97	0.991		1-2	458
2	0.8691	1.2	0.9897		2-3	434
3	0.8688	1.42	0.9885		3-4	387
4	0.8655	1.65	0.9873		4-5	302
5	0.8732	1.83	0.9863		5-6	296
6	0.8708	2.01	0.9853		6-7	271
7	0.8492	2.2	0.9843		7-8	146
8	0.8401	2.41	0.9836		8-9	35.6
9	0.6501	2.47	0.9833		9-10	30.7
10	0.5693	2.55	0.983			

Table 4.5 shows that the voltage profile and THD are similar to Case 1. This indicates that moderate afternoon EV charging has little extra impact. Network stress is low, and branch losses are manageable.

Table 4. 6 Case 4 – Afternoon Maximum EV Scenario

CASE 4						
NODE	PF	THD (phase A)	voltage(pu)		Branch	power loss(W)
1	0.8824	1.18	0.9878		1-2	458
2	0.882	1.45	0.986		2-3	434
3	0.8826	1.72	0.9842		3-4	387
4	0.8816	2	0.9825		4-5	302
5	0.8861	2.24	0.981		5-6	296
6	0.8856	2.49	0.9796		6-7	271
7	0.8769	2.75	0.9781		7-8	146
8	0.8741	3.04	0.977		8-9	35.6
9	0.7136	3.04	0.9766		9-10	30.7
10	0.6429	3.06	0.9764			

Table 4.6 shows a slight decline in voltage and THD compared to Case 2. This change reflects the highest afternoon EV load. Losses along feeder branches increase, demonstrating the impact of concentrated charging times.

Table 4. 7 Case 5 – Evening Normal EV Scenario

CASE 5						
NODE	PF	THD (phase A)	voltage(pu)		Branch	power loss(W)
1	0.8687	1.29	0.9874		1-2	796
2	0.8679	1.59	0.9855		2-3	763
3	0.8684	1.89	0.9836		3-4	701
4	0.8668	2.19	0.9818		4-5	596
5	0.8727	2.46	0.9802		5-6	589
6	0.8719	2.74	0.9787		6-7	554
7	0.8604	3.03	0.9772		7-8	368
8	0.8567	3.34	0.9759		8-9	35
9	0.6126	3.37	0.9755		9-10	30
10	0.5446	3.41	0.9751			

Table 4.7 shows further voltage drop during evening normal charging with 43.02% EV penetration. THD increases slightly to about 3.4%. Branch losses rise on heavily loaded lines, which indicates moderate evening stress.

Table 4. 8 Case 6 – Evening Maximum EV Scenario

CASE 6						
NODE	PF	THD (phase A)	voltage(pu)		Branch	power loss(W)
1	0.8695	1.29	0.9834		1-2	1399
2	0.8699	1.59	0.9808		2-3	1354
3	0.8712	1.89	0.9783		3-4	1266
4	0.8711	2.2	0.9759		4-5	1096
5	0.8742	2.48	0.9737		5-6	1084
6	0.8746	2.77	0.9715		6-7	1033
7	0.8684	3.07	0.9694		7-8	747
8	0.8672	3.39	0.9675		8-9	31
9	0.7179	3.39	0.9672		9-10	26.3
10	0.6488	3.38	0.9669			

Table 4.8 shows voltage and PF decreasing further while THD approaches around 3.4–3.5%. Branch losses increase sharply, showing high evening EV load (66.93%) impacts feeder stability.

Table 4. 9 Case 7 – Night Normal EV Scenario

CASE 7						
NODE	PF	THD (phase A)	voltage(pu)		Branch	power loss(W)
1	0.8782	1.29	0.984		1-2	1386
2	0.8786	1.59	0.9816		2-3	1342
3	0.88	1.9	0.9792		3-4	1256
4	0.88	2.2	0.9769		4-5	1122
5	0.8861	2.48	0.9748		5-6	1111
6	0.8867	2.77	0.9727		6-7	1061
7	0.882	3.07	0.9707		7-8	778
8	0.8813	3.39	0.9689		8-9	23
9	0.7679	3.38	0.9687		9-10	21
10	0.6606	3.38	0.9686			

Table 4.9 shows continued voltage drop (~0.968 pu at node 10) and elevated THD (~3.38%). Losses are concentrated in early branches; PF shows growing network stress during night.

Table 4.10 shows the highest EV load before full saturation (84.85%). Voltage dips below 0.964 pu at far nodes, THD rises to ~3.85%, and branch losses are high. PF remains ~0.87–0.88. This scenario shows the critical/optimal condition for studying future EV expansion. Similarly, Table

4.11 shows the current THD for each node and harmonics loss for each branch suggesting that the impact of controlled EV charger on harmonic loss is minimum.

Table 4. 10 Case 8 – Night Maximum EV Realistic Scenario

CASE 8						
NODE	PF	THD (phase A)	voltage(pu)		Branch	power loss(W)
1	0.8728	1.44	0.9816		1-2	1759
2	0.8736	1.77	0.9787		2-3	1709
3	0.8753	2.11	0.976		3-4	1612
4	0.8758	2.46	0.9733		4-5	1445
5	0.8814	2.79	0.9708		5-6	1433
6	0.8823	3.13	0.9684		6-7	1376
7	0.8785	3.47	0.966		7-8	1051
8	0.8783	3.85	0.9639		8-9	35.18
9	0.7207	3.84	0.9636		9-10	30.6
10	0.6526	3.84	0.9633			

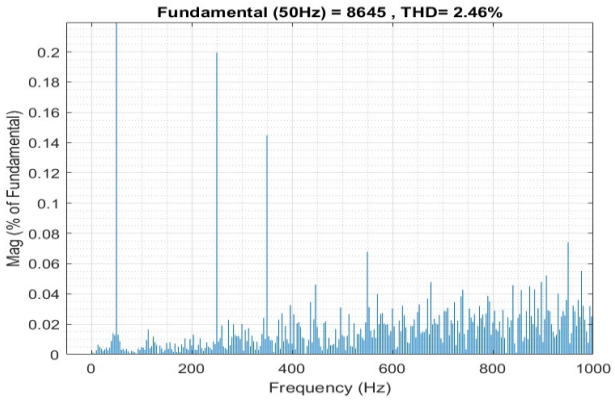

Figure 4. 3 THD at node 4 for case 8

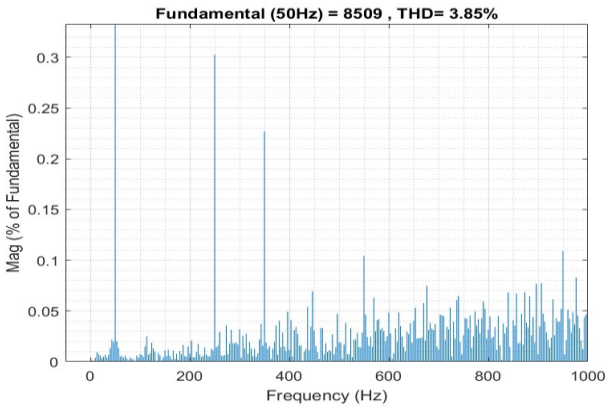

Figure 4. 4 THD at node 8 for case 8

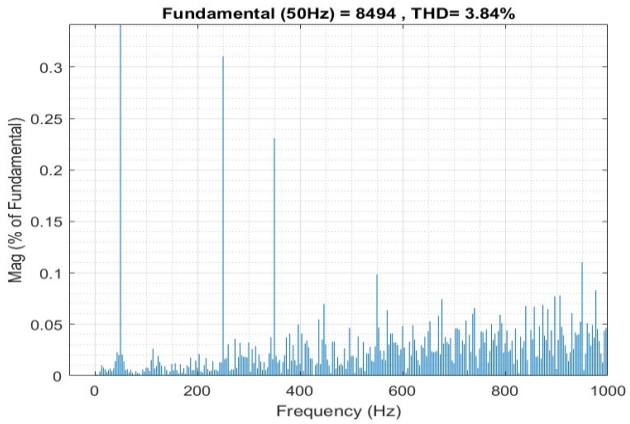

Figure 4. 5 THD at node 10 for case 8

Table 4. 11 Case 8- Harmonic loss calculation

CASE 8									
Node	THD %	Fundamental peak	5th % harmonic	7th % harmonic		Branch	Total power loss (W)	harmonic loss (W)	% harmonic loss
1	1.33	679.3	0.87	0.39		1 2	1759	0.32	0.02
2	1.35	668.8	0.88	0.4		2 3	1709	0.32	0.02
3	1.36	664.5	0.89	0.4		3 4	1612	0.31	0.02
4	1.39	652	0.91	0.41		4 5	1445	0.28	0.02
5	1.4	620.6	0.88	0.43		5 6	1433	0.29	0.02
6	1.42	612.3	0.89	0.44		6 7	1376	0.33	0.02
7	1.54	571	0.96	0.47		7 8	1051	0.26	0.02
8	1.58	558.7	0.98	0.49		8 9	35.18	0.01	0.03
9	1.61	191.1	0.87	0.51		9 10	30.6	0.01	0.03
10	1.67	184.7	0.9	0.53					

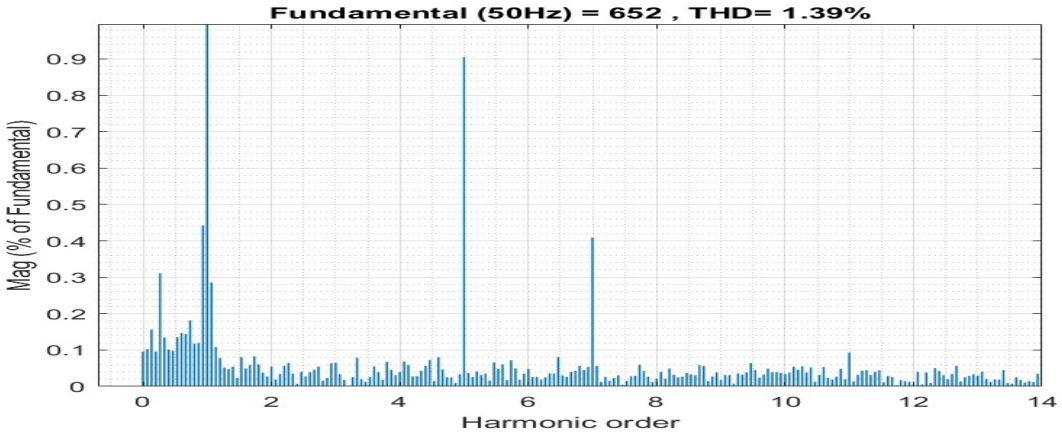

Figure 4. 6 Current THD at node 4 for case 8

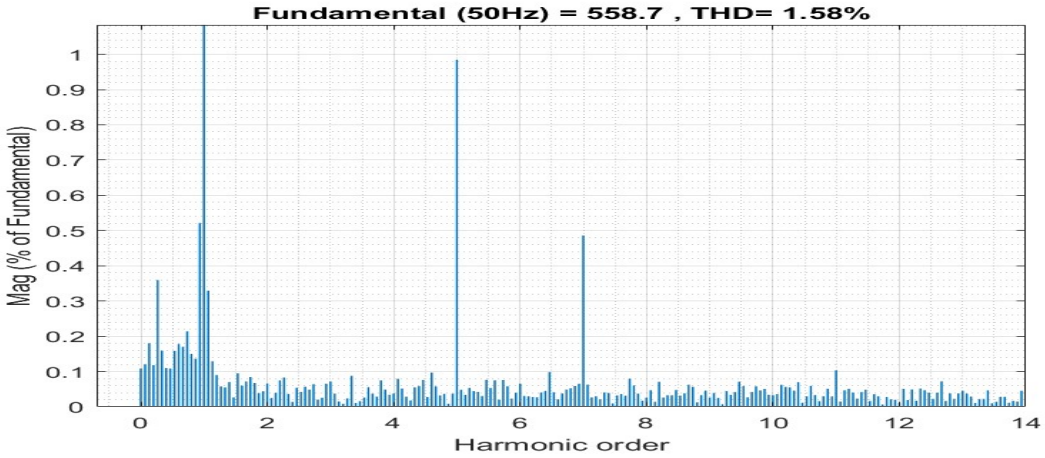

Figure 4. 7 Current THD at node 8 for case

From equation 2.34,

$$P_{harm} = \frac{Ptotal}{1+THD^2} \times THD^2$$

For case 8 at node 1,

P_{total} = 1759 W

THD = 1.33 % = 0.0133

Then,

$$P_{harm} = \frac{1750}{1+0.0133^2} \times 0.0133^2$$

P_{harm} = 0.311 W

Table 4. 12 Case 9 – Full Load EV Scenario

CASE 9- fully loaded						
NODE	PF	THD (phase A)	voltage(pu)		Branch	power loss(W)
1	0.8799	1.63	0.9808		1-2	2075
2	0.8811	2	0.9779		2-3	2024
3	0.8829	2.38	0.975		3-4	1920
4	0.8838	2.76	0.9723		4-5	1710
5	0.8876	3.11	0.9698		5-6	1697
6	0.888	3.48	0.9673		6-7	1636
7	0.8862	3.86	0.9649		7-8	1280
8	0.8865	4.26	0.9627		8-9	41
9	0.7191	4.25	0.9624		9-10	36
10	0.6513	4.24	0.9621			

Table 4.12 shows voltage drops further (~0.962 pu at node 10), THD exceeds 4%, and losses peak, indicating the feeder is fully loaded. PF slightly decreases but stays above 0.65 at critical nodes. This scenario shows the worst-case condition for comparison.

4.5 Future Expansion

The impact of future EV expansion is analyzed under two scenarios: crowded and distributed. Both scenarios consider additional EV chargers added to the feeder network as described in Section 3.5.2 and 3.5.3.

4.5.1 Crowded Case

Additional chargers are added to existing EV locations, representing high EV penetration. The results are summarized in tables and figures for voltage profiles, power loss, power factor, and THD.

Table 4. 13 Crowded Future Expansion – High EV Penetration at Case 8

NODE	PF	THD (phase A)	voltage(pu)
1	0.8756	1.98	0.9744
2	0.8779	2.43	0.9705
3	0.8807	2.89	0.9666
4	0.8827	3.35	0.9629
5	0.8877	3.79	0.9594
6	0.89	4.24	0.956
7	0.8897	4.7	0.9527
8	0.885	5.12	0.9502
9	0.8304	5.15	0.9495
10	0.6148	5.17	0.9492

Branch	power loss(W)
1 2	3849
2 3	3783
3 4	3645
4 5	3391
5 6	3370
6 7	3281
7 8	2057
8 9	212
9 10	55

Table 4. 14 Crowded case - Harmonic loss calculation

Crowded case									
Node	THD %	Fundamental peak	5th % harmonic	7th % harmonic		Branch	Total power loss (W)	harmonic loss (W)	% harmonic loss
1	1.81	792	0.7	0.47		1 2	3849	1.3	0.03
2	1.84	781	0.71	0.47		2 3	3783	1.29	0.03
3	1.85	777	0.72	0.48		3 4	3645	1.08	0.03
4	1.72	651	0.97	0.52		4 5	3391	1.01	0.03
5	1.73	619	0.92	0.54		5 6	3370	1.04	0.03
6	1.76	611	0.93	0.54		6 7	3281	1.18	0.04
7	1.9	569	1	0.59		7 8	2057	0.78	0.04
8	1.95	556	1.02	0.6		8 9	212	0.19	0.09
9	3.02	156	0.95	0.53		9 10	55	0.22	0.4
10	6.37	36	1.45	0.4					

Table 4.13 shows additional chargers added at existing stations, increasing THD to ~5.17% and voltage dropping to ~0.949 pu at node 10. Branch losses rise sharply (>3800 W on main lines). PF slightly decreases but remains acceptable. This scenario shows the impact of concentrated future EV growth. Similarly, Table 4.14 shows the current THD at each node and harmonic power loss at each branch suggesting that the current THD exceeds the 5% at node 10.

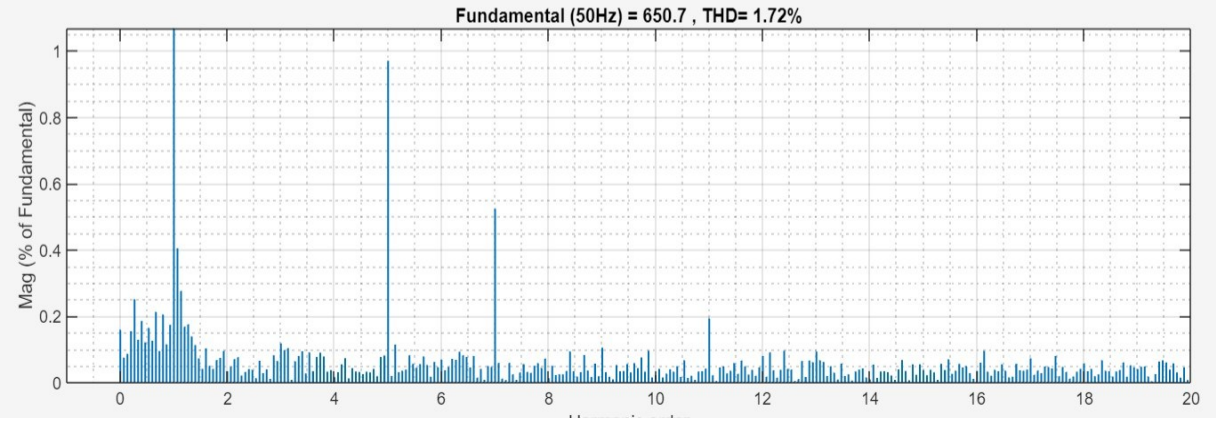

Figure 4. 8 Current THD at node 4 for crowded case

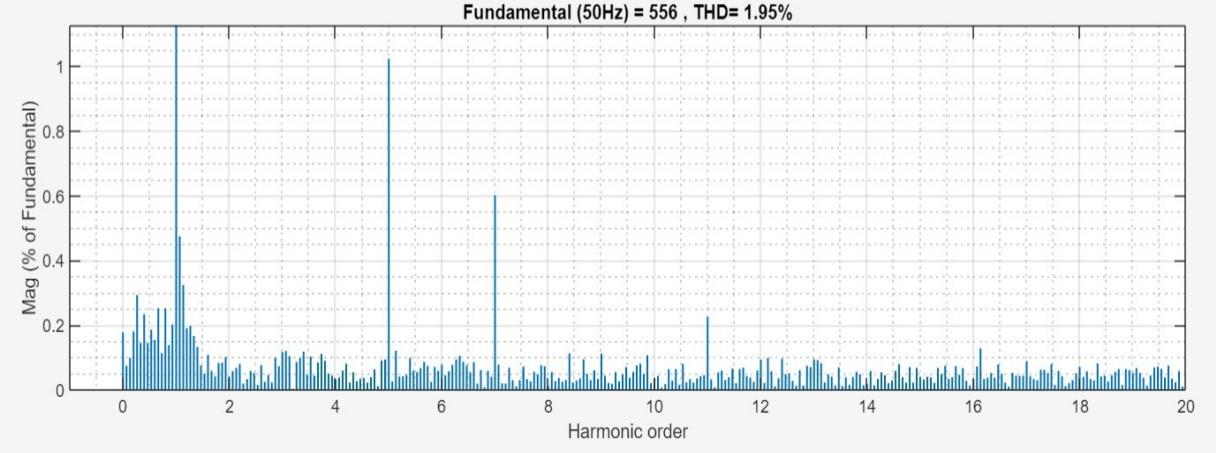

Figure 4. 9 Current THD at node 8 for crowded case

4.5.2 Distributed Case

New EV chargers are added at nodes farther from existing stations to represent distributed future EV penetration. Results are summarized similarly.

Table 4. 15 Distributed Future Expansion – Distributed EV Charging at case 8

NODE	PF	THD (phase A)	voltage(pu)
1	0.8756	2.17	0.9689
2	0.8785	2.67	0.9642
3	0.8818	3.17	0.9596
4	0.883	3.61	0.9558
5	0.888	4.05	0.9523
6	0.8903	4.51	0.9489
7	0.8838	4.99	0.9456
8	0.884	5.42	0.9435
9	0.6565	5.42	0.9432
10	0.6481	5.43	0.9429
11	0.9064	4.99	0.9456
12	0.9067	5.2	0.9437

Branch	power loss(W)
1-2	4654
2-3	4580
3-4	3550
4-5	3290
5-6	3268
6-7	3178
7-8	1463
8-9	52
9-10	48
7-11	461
11-12	433

Table 4. 16 Distributed case - Harmonic loss calculation

Distributed case									
Node	THD %	Fundamental peak	5th % harmonic	7th % harmonic		Branch	Total power loss (W)	harmonic loss (W)	% harmonic loss
1	1.62	876	0.65	0.35		1 2	4654	1.25	0.03
2	1.64	866	0.65	0.35		2 3	4580	1.25	0.03
3	1.65	861	0.66	0.35		3 4	3550	0.98	0.03
4	1.66	734	1.06	0.53		4 5	3290	0.92	0.03
5	1.67	703	1	0.55		5 6	3268	0.93	0.03
6	1.69	694	1.01	0.56		6 7	3178	1.47	0.05
7	2.15	456	1.06	0.6		7 8	1463	0.71	0.05
8	2.21	443	1.09	0.62		8 9	52	0.16	0.31
9	5.49	44.23	1.1	0.43		9 10	48	0.21	0.44
10	6.65	37	1.35	0.53		7 11	461	0.31	0.07
11	2.58	213	1.04	0.55		11 12	433	0.31	0.07
12	2.69	205	1.09	0.57					

Table 4.15 shows additional chargers distributed across new nodes. THD is slightly higher (~5.43%), voltage dips to ~0.942 pu, and branch losses are moderate on new lines. PF is slightly higher than crowded case in far nodes. This scenario shows distributed charging mitigates network stress compared to concentrated growth. Similarly, Table 4.16 shows the current THD at each node and harmonic loss at each branch suggesting that the harmonic loss increases along with the EV penetration and the current THD at end node 9 and 10 exceeds 5%.

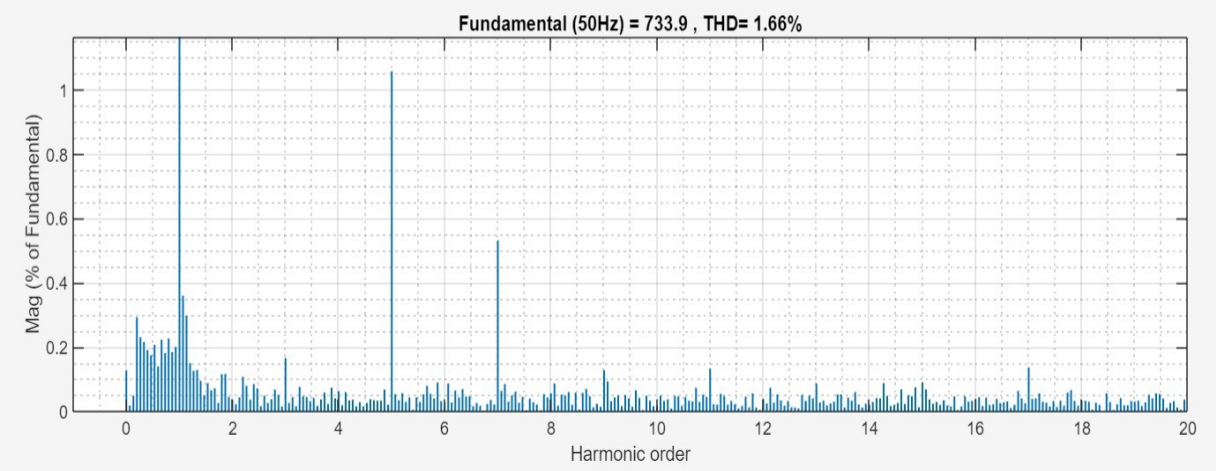

Figure 4. 10 Current THD at node 4 for distributed case

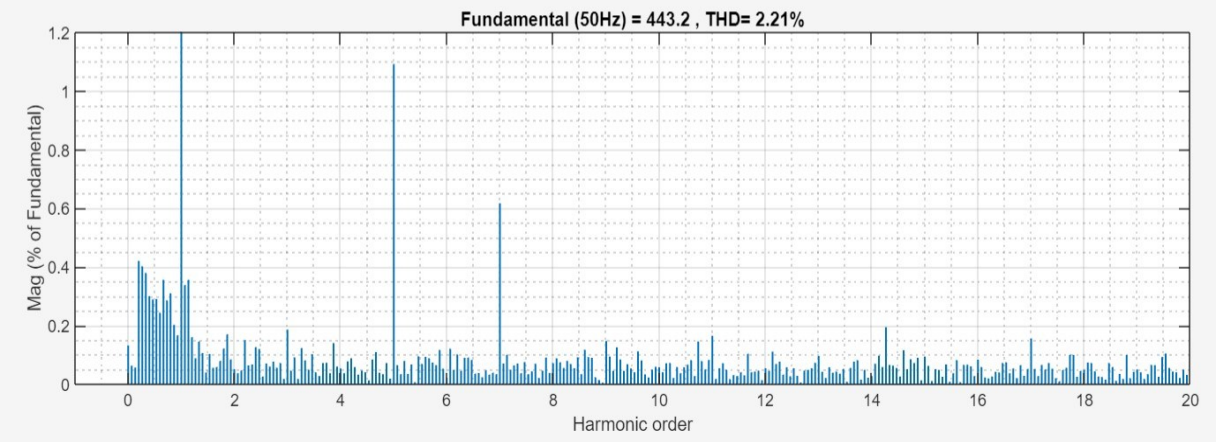

Figure 4. 11 Current THD at node 8 for distributed case

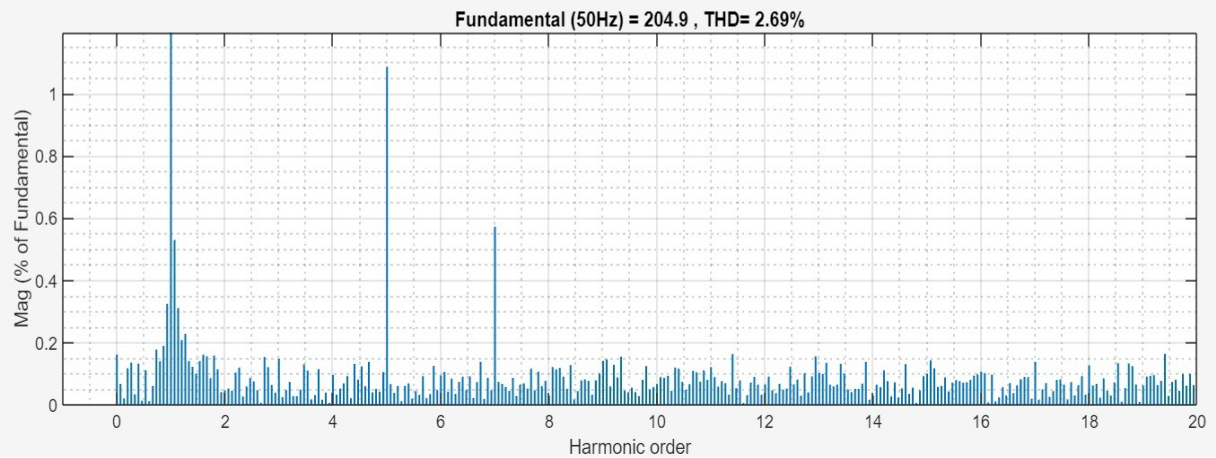

Figure 4. 12 Current THD at node 12 for distributed case

4.6 Comparison Analysis

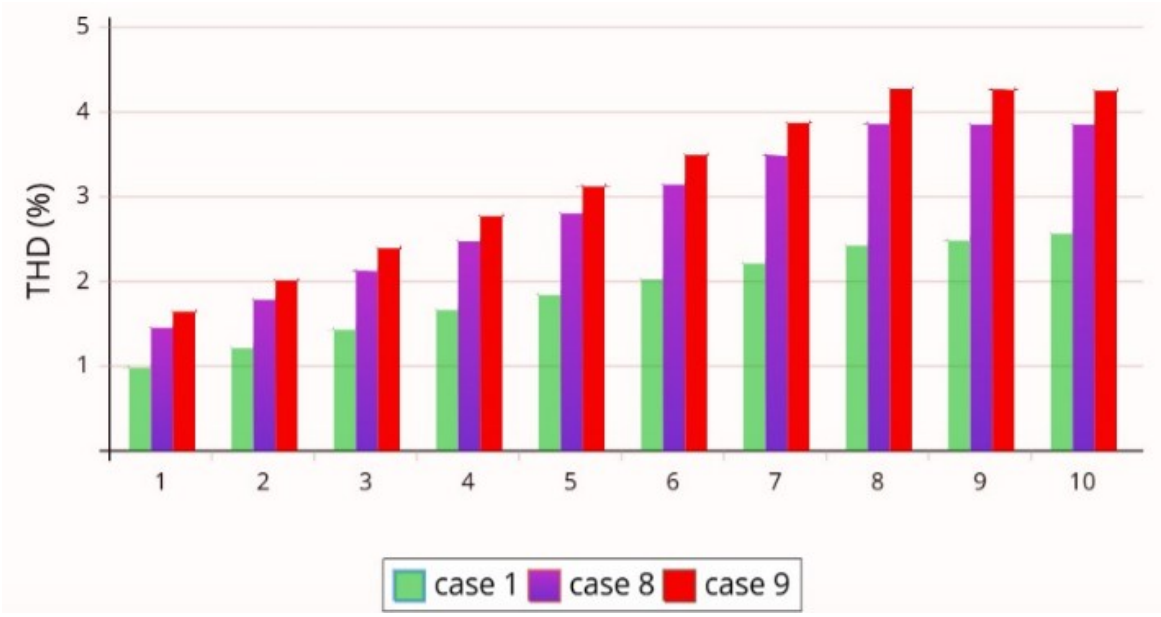

Figure 4. 13 THD Comparison across nodes

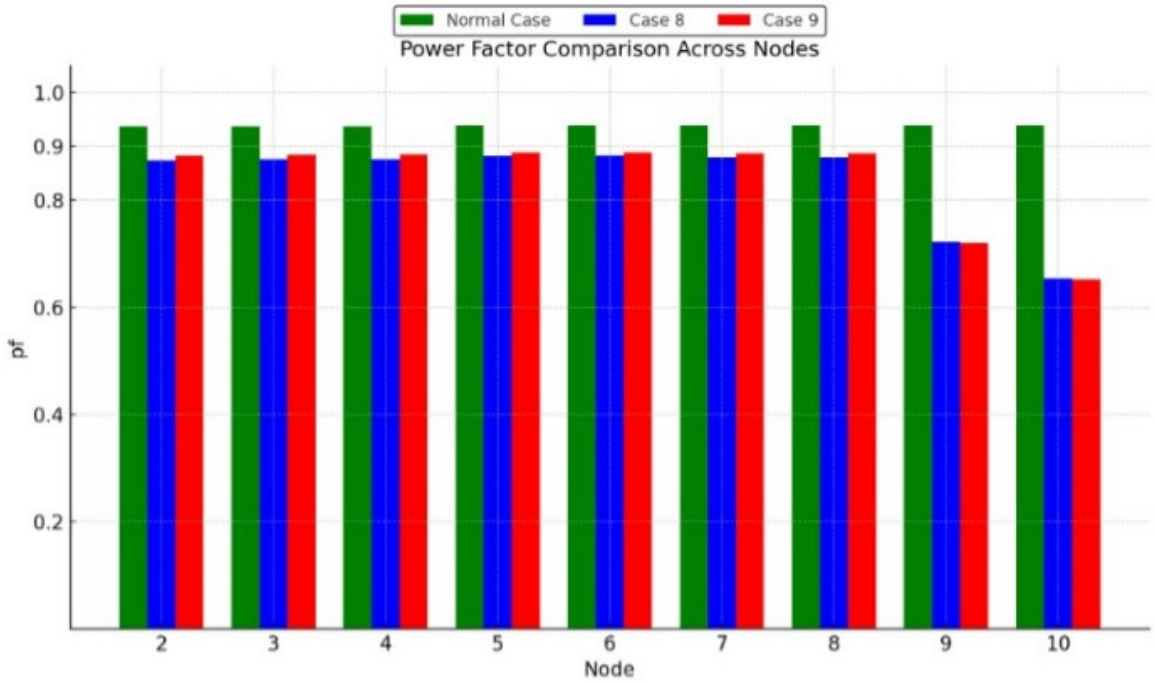

Figure 4. 14 Power factor Comparison across nodes

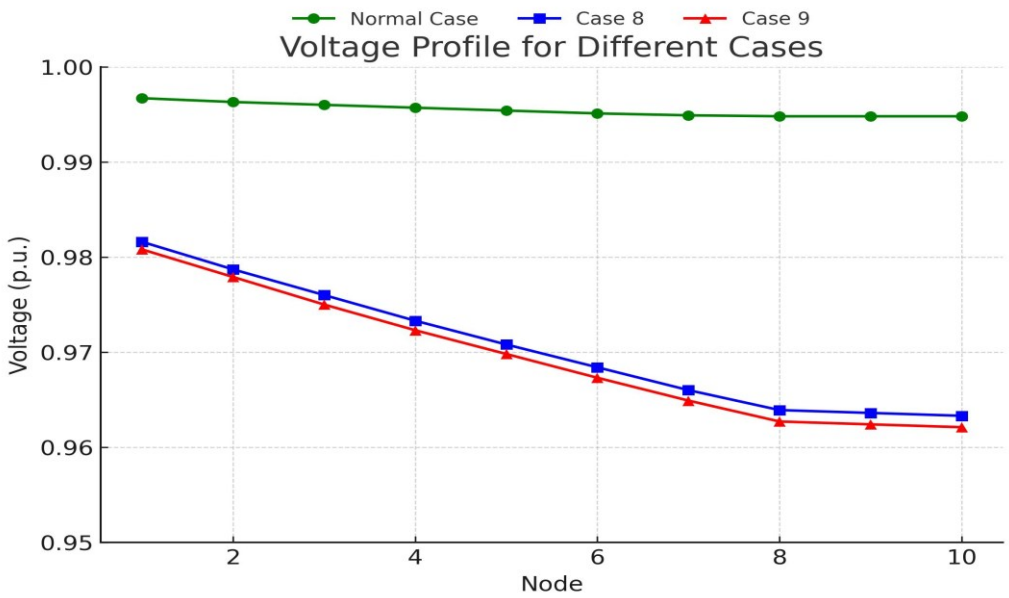

Figure 4. 15 Voltage in pu Comparison across nodes

Figure 4.13 shows the bar graph of THD across nodes for case 1, case 8 and case 10. The THD level increases from case 1 to case 9 within the case and it also rises as we move from lower node to higher node.

Similarly, Figure 4.14 shows the bar graph of power factor across nodes for normal case, case 8 and case 9. For each nodes, the power factor is higher for normal case and almost same for case 8 and case 9. And power factor decreases drastically at node 8 and 9 for case 8 and case 9, it is because there is only EV charging station connected at node 9 and the grid stability also becomes weaker for end nodes due to increase in impedance.

In the same way, Figure 4.15 shows the line graph of voltage in pu across nodes for normal case, case 8 and case 9. The voltage is almost 1pu for normal case in each node. The voltage decreases progressively for case 8 and case 9 from lower node to the higher node.

4.7 Additional EV Integration Capacity Study

Initially, the MATLAB Simulation was performed with active and reactive power only for residential loads without considering nonlinear loads as shown in Table 4.1. However, there is always some nonlinear current drawn by nonlinear load which are present in real time practical

cases. So, to compromise this, base THD of 1.5% and 2% are taken into consideration to find the actual additional EV chargers that can be integrated into the Sanepa Feeder.

Table 4. 17 Hosting capacity with base THD

Scenario	Current additional EV load (kW)	THD W/O base (%)	Max THD allowed (%)	Max EV load with 1.5% base (kW)	Max EV load with 2% base (kW)
Crowded	600	5.17	5	553	532
Distributed	840	5.37	5	746	717

4.7.1 EV Harmonic Contribution and Maximum Allowable Load Calculation

1. Governing Formulas

A. Maximum Allowable EV Harmonic Contribution

THD limit = 5%

Formula:

$$THD_{EV-max} = \sqrt{{THD_{limit}}^2 + {THD_{base}}^2}$$

B. Scaling the Maximum EV Load

$$P_{EV-max} = P \times \frac{THD_{EV-max}}{THD_{voltage}}$$

2. Verification: Crowded Scenario

Given:

P = 600 kW

THD = 5.37%

Case A: 1.5% Base THD

$THD_{EV-max} = \sqrt{25 - 2.25} = 4.7697\%$

$P_{EV-max} = 600 * \frac{4.7697}{5.17}$

= 553.5 kW

Case B: 2.0% Base THD

$THD_{EV-max} = \sqrt{25 - 4} = 4.5826\%$

$$P_{EV-max} = 600 * \frac{4.5826}{5.17}$$
$$= 531.8 \text{ kW}$$

3. Verification: Distributed Scenario

Given:

P = 840 kW

THD = 5.17%

Case A: 1.5% Base THD

$THD_{EV-max} = \sqrt{25 - 2.25} = 4.7697\%$

$$P_{EV-max} = 840 * \frac{4.7697}{5.37}$$
$$= 746.1 \text{ kW}$$

Case B: 2.0% Base THD

$THD_{EV-max} = \sqrt{25 - 4} = 4.5826\%$

$$P_{EV-max} = 840 * \frac{4.5826}{5.37}$$
$$= 716.8 \text{ kW}$$

4.8 Result Discussion

The paper investigates the impact of electric vehicle fast charging stations on the Sanepa medium-voltage distribution feeder. Simulation analysis was carried out under several operational scenarios to assess the changes in power factor, total harmonic distortion, node voltage, and power losses for the existing and projected EV penetration levels. Analyses were performed using real field data from chargers like BYD, MG, Hyundai, NEA, and Sajha Yatayat. Equivalent charger modeling was used, resulting in high-capacity chargers being modeled using simplified equivalents. For example, a number of smaller chargers were aggregated together in order to simplify the simulation. Comparing single and dual configurations showed that the error in power factor, THD, and voltage is minimal, confirming that this kind of modeling is appropriate.

The base case scenario represents the existing operating condition without EV charging load, and it serves as a benchmark for node voltage and power loss. For subsequent studies, nine EV charging scenarios were analyzed: Cases 1-8 are practical operational conditions according to field data, while Case 9 is a hypothetical full EV penetration case. Computer simulation results show a clear trend of increased power loss, THD, and deterioration of power factor due to higher integrations of EV chargers. However, the study does point out that the magnitudes of the current THD will remain comparatively moderate across the study cases. This is mainly because of the operational characteristics of the EV chargers, which function under controlled CC and CV modes. These control schemes naturally regulate the input current waveform and hence can prevent excessive harmonic injection. As a direct result of the suppressed current THD, the harmonic component of the power loss is found to be minimal. Detailed analysis has verified that the harmonic loss percentage can be sufficiently low and generally below 1% across all nodes, indicating that while waveform distortion does occur, the particular thermal stress contributed by harmonics is negligible when compared to the fundamental load.

Typical medium-voltage feeders of 8 to 12 km long usually have a Base THD in the range of 1.5% to 2.5% from existing nonlinear loads like power supplies, LEDs, UPS systems, and variable frequency drives. When these background harmonics are included, the hosting capacity of the feeder changes dramatically compared to ideal simulation conditions. In the crowded deployment scenario, 600 kW of EV load was injected, which, through raw simulation, returned a THD of 5.17%. However, maintaining compliance with the IEEE 519 limit of 5% when accounting for a 1.5% Base THD, the maximum allowable EV load becomes approximately 553 kW. If the background distortion is higher at 2%, the allowable load decreases even further to 532 kW. Meanwhile, the scenario of distributed deployment presents much better hosting capacity. Although this simulation for 840 kW of distributed load showed a raw THD of 5.37%, the network handles that load in a much better manner than in the crowded case. When adjusted for a 1.5% Base THD, up to 746 kW of distributed EV load can safely be supported on the feeder. Considering an increased Base THD of 2%, the permissible load remains substantial at 717 kW. This clearly sets up a very significant advantage of spatial distribution; spreading rather than crowding the chargers across the network enables the feeder to support some additional 200 kW or so of load while still staying within the same power quality constraints. It is worth

mentioning at this point that the precise estimate of Base THD is crucial for compliance purposes, because neglecting the background noise could greatly overestimate the capacity of the grid. The analysis also identified some specific weak points in the grid structure: In both crowded and distributed scenarios, the nodes at the end of the feeder show high current THD values disproportionately. This is because the fundamental current at these end nodes is small, and thus even a moderate harmonic injection from EV chargers leads to a high harmonic-to-fundamental current ratio. Spectral analysis showed that the dominant contributions to this distortion come from the 5th and 7th harmonic orders. When the feeder was evaluated against IEEE 519 standards, it can be observed that, due to the relatively low system short-circuit ratio, a maximum allowable THD of 5% can be supported. While the realistic Cases (Cases 1–8) are generally within these limits, the high-penetration cases reach or exceed this limit, particularly towards the ends of feeders. Thus, although the feeder at Sanepa would still be operating within acceptable limits, strategic distributed placement and potential harmonic mitigation would be necessary to maximize hosting capacity and prevent any future degradation of power quality.

CHAPTER 5: CONCLUSION AND RECOMMENDATION

5.1 Conclusion

This work examines the harmonic and power quality impact caused by EV charging on the Sanepa medium-voltage distribution feeder; it validates an equivalent charger modelling approach and presents simulation results. The results confirm that high EV penetration increases system distortion and losses, but the system operates within IEEE 519 compliance (THD <5%) up to the realistic Case 8, mainly because modern chargers make use of controlled CC/CV operational modes that keep Current THD low, hence harmonic power losses will be negligible (below 1%) relative to the total losses. However, significant vulnerabilities are identified at the feeder's end-of-line nodes where the low fundamental currents cause localized Current THD spikes over 6%, dominated by the 5th and 7th harmonic orders. Importantly, future hosting capacity is highly dependent on charger location and background noise: accounting for a realistic Base THD (1.5–2%), crowded deployment is limited to approximately 532–553 kW of new load, while in distributed-uncrowded deployment, the capacity significantly improves, and 717–746 kW of additional load is allowed while the constraint on power quality is maintained. This underlines that in the current framework, the most effective measure to maximize feeder hosting capacity is the strategic distribution of chargers.

5.2 Recommendation

Recommendation for further work based on findings obtained from this thesis study include the following, which can support the future planning of sustainable integration of EV charging stations in the Sanepa feeder:

1. **Incorporate Future Base Load Growth**

   As such the investment in EV charging points will be phased over time and the base feeder load will increase. The anticipated increase in load from the utility data center must be considered in future studies for a realistic feeder condition which represents actual commissioning times.

2. Assess Compensation Techniques When THD Nears IEEE Limits

Investigations based on the SAPF compensation plant might be conducted if voltage THD attained or exceeded 5% as per IEEE standards under the future condition. Their placement, performance and compatibility will need to be evaluated in order to avoid instant investment into infrastructure for power quality.

3. Conduct in-depth analysis of the siting for distributed charger locations

On the other hand, the location of individual chargers has to be studied through several case studies to ensure they meet IEEE power quality levels and that as well maximize the use of existing infrastructure without over depending expensive compensation methods.

4. Integrate Realistic Residential and Single-Phase EV Charging Patterns

Future models should include typical urban charging conditions like single-phase loads from residences and two-wheeler EV charging. Seasonal variations and time-of-day load behavior should also be included for improved accuracy.

5. Assess the impact of offline or under-maintenance chargers

Some chargers remain inactive due to faults or maintenance. Future work should address whether such units will be restored or permanently removed and study the resulting changes on the voltage profiles, losses, and harmonic levels.

6. Support utility planning and policy development

These expanded findings should be used by utilities and policymakers for the purpose of guiding optimum EV charger deployment, determining priority reinforcement points, and ensuring reliable, power-quality-compliant operation as EV adoption increases.

REFERENCES

[1] Zhiyun Li, "A Review of the Current Status of Global Electric Vehicle Charging Infrastructure Development," *Internation journal of Global Economics and Management*, vol. 3, 2024.

[2] P. Biswas *et al.*, "Vehicle to Grid: Technology, Charging Station, Power Transmission, Communication Standards, Techno-Economic Analysis,
Challenges, and Recommendations," Mar. 01, 2025, *Multidisciplinary Digital Publishing Institute (MDPI)*. doi:10.3390/wevj16030142.

[3] J. Su, T. T. Lie, and R. Zamora, "Integration of Electric Vehicles in Distribution Network Considering Dynamic Power Imbalance Issue," *IEEE Trans Ind Appl*, vol. 56, no. 5, pp. 5913–5923, Sep. 2020, doi: 10.1109/TIA.2020.2990106.

[4] E. F. and M. M. A. Fuchs, *POWER QUALITY IN POWER SYSTEMS AND ELECTRICAL MACHINES*. Academic press, 2011.

[5] "IEEE Standard for Shunt Power Capacitors," *IEEE Std 18-2002 (Revision of IEEE Std 18-1992)*, pp. 1–20, 2002.

[6] H. Li, F. Zhuo, Z. Wang, W. Lei, and L. Wu, "A novel time-domain current detection algorithm for shunt active power filters," *IEEE Transactions on Power Systems*, vol. 20, no. 2, pp. 644–651, May 2005, doi: 10.1109/TPWRS.2005.846215.

[7] Sabir Ouchen and Jean-Paul Gaubert and Heinrich Steinhart and Achour Betka,

"Energy quality improvement of three-phase shunt active power filter under different voltage conditions based on predictive direct power control with disturbance rejection principle," *Math Compute Simul*, vol. 158, no. 0378–4754, pp. 506–519, 2019.

[8] Z. Salam, A. Jusoh, and T. P. Cheng, "Harmonics mitigation using active power filter: A technological review," 2006.

[9] R. K. Nepal, B. Khanal, S. Khatiwada, N. Bhandari, B. Rijal, R. Karmacharya, and A. Thapa, "Compensation for reactive power and harmonic current drawn by a non-linear load in a PV–micro hydro grid," arXiv preprint arXiv:2406.05342, Jun. 2024.

[10] M. Y. and M. V. and P. S. and C. V. and S. I. Artemenko, "Modified

Instantaneous Power Theory for Three-Phase Four-Wire Power Systems," *2019 IEEE 39th International Conference on Electronics and Nanotechnology (ELNANO)*, pp. 600–605, 2019.

[11] Y. K. K. F. A. N. Hirofumi Akagi, "Generalized theory of instantaneous reactive power and its application," 1983.

[12] *2019 IEEE 39th International Conference on Electronics and Nanotechnology (ELNANO): conference proceedings: April 16-18, 2019, Kyiv, Ukraine*. IEEE, 2019.

[13] H. Akagi, Y. Kanazawa, and A. Nabae, "Instantaneous Reactive Power Compensators Comprising Switching Devices without Energy Storage Components," *IEEE Trans Ind Appl*, vol. 20, no. 3.

[14] S. Buso, L. Malesani, and P. Mattavelli, "Comparison of Current Control Techniques for Active Filter Applications," *IEEE TRANSACTIONS ON INDUSTRIAL ELECTRONICS*, vol. 45, no. 5, 1998.

[15] M. A. Rahman, T. S. Radwan, A. M. Osheiba, and A. E. Lashine, "Analysis of Current Controllers for Voltage-Source Inverter," *IEEE TRANSACTIONS ON INDUSTRIAL ELECTRONICS*, vol. 44, no. 4, p. 477, 1997.

[16] H. Mao, X. Yang, Z. Chen, and Z. Wang, "A hysteresis current controller for single-phase three-level voltage source inverters," *IEEE Trans Power Electron*, vol. 27, no. 7, pp. 3330–3339, 2012, doi: 10.1109/TPEL.2011.2181419.

[17] K. M. Rahman, M. Rezwan Khan, M. A. Choudhury, and M. A. Rahman, "Variable-Band Hysteresis Current Controllers for PWM Voltage-Source Inverters," *IEEE Trans Power Electron*, vol. 12, no. 6, 1997.

[18] S. H. Saeed, *Automatic Control System*, Revised. S. K. Kataria & Sons, 2008.

[19] A. Srivastava and S. Saravanan, "Harmonic mitigation using optimal active power filter for the improvement of power quality for a electric vehicle changing station," *e-Prime - Advances in Electrical Engineering, Electronics and Energy*, vol. 8, Jun. 2024, doi: 10.1016/j.prime.2024.100527.

[20] N. Zhou, J. Wang, Q. Wang, N. Wei, and X. Lou, "Capacity calculation of shunt active power filters for electric vehicle charging stations based on harmonic parameter

estimation and analytical modeling," *Energies (Basel)*, vol. 7, no. 8, pp. 5425–5443, 2014, doi: 10.3390/en7085425.

[21] Y. and Y. D. and Z. G. and W. H. and Z. J. Zhang, "Harmonic Analysis of EV Charging Station Based on Measured Data," *2020 IEEE/IAS Industrial and Commercial Power System Asia (I&CPS Asia)*, pp. 475–480, 2020.

[22] M. Senol *et al.*, "Harmonics Measurement, Analysis, and Impact Assessment of Multiple Electric Vehicle Smart Charging," *IEEE Open Journal of Vehicular Technology*, 2024, doi: 10.1109/OJVT.2024.3505778.

[23] A. Mariscotti, "Harmonic and Supraharmonic Emissions of Plug-In Electric Vehicle Chargers," *Smart Cities*, vol. 5, no. 2, pp. 496–521, Jun. 2022, doi: 10.3390/smartcities5020027.

[24] D. Committee of the IEEE Power and E. Society, "IEEE Recommended Practice and Requirements for Harmonic Control in Electric Power Systems Sponsored by the Transmission and Distribution Committee IEEE Power and Energy Society."

[25] M. J. Ghorbani and H. Mokhtari, "Impact of Harmonics on Power Quality and Losses in Power Distribution Systems," International Journal of Electrical and Computer Engineering (IJECE), vol. 5, no. 1, pp. 166–174, Feb. 2015.

[26] T. A. H. Alghamdi, Analysis and Solutions of Power Harmonics in Medium Voltage Distribution Networks, Ph.D. dissertation, Cardiff Univ., 2022.

APPENDIX

Appendix A: (Simulink Model)

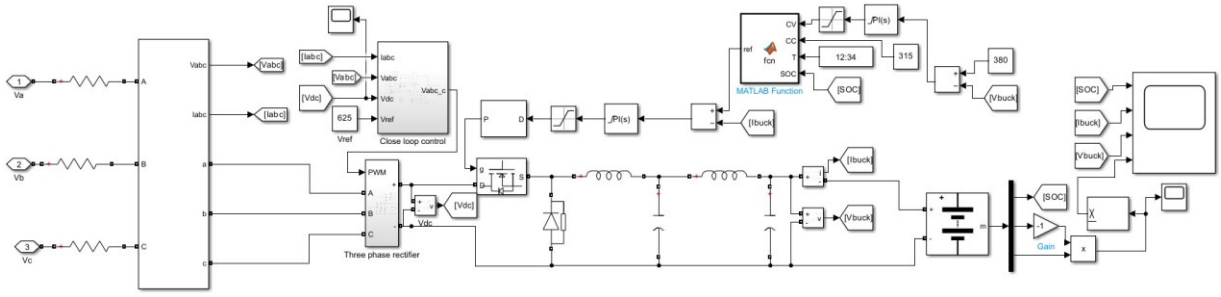

Figure A. 1 Simulation model of EV charger

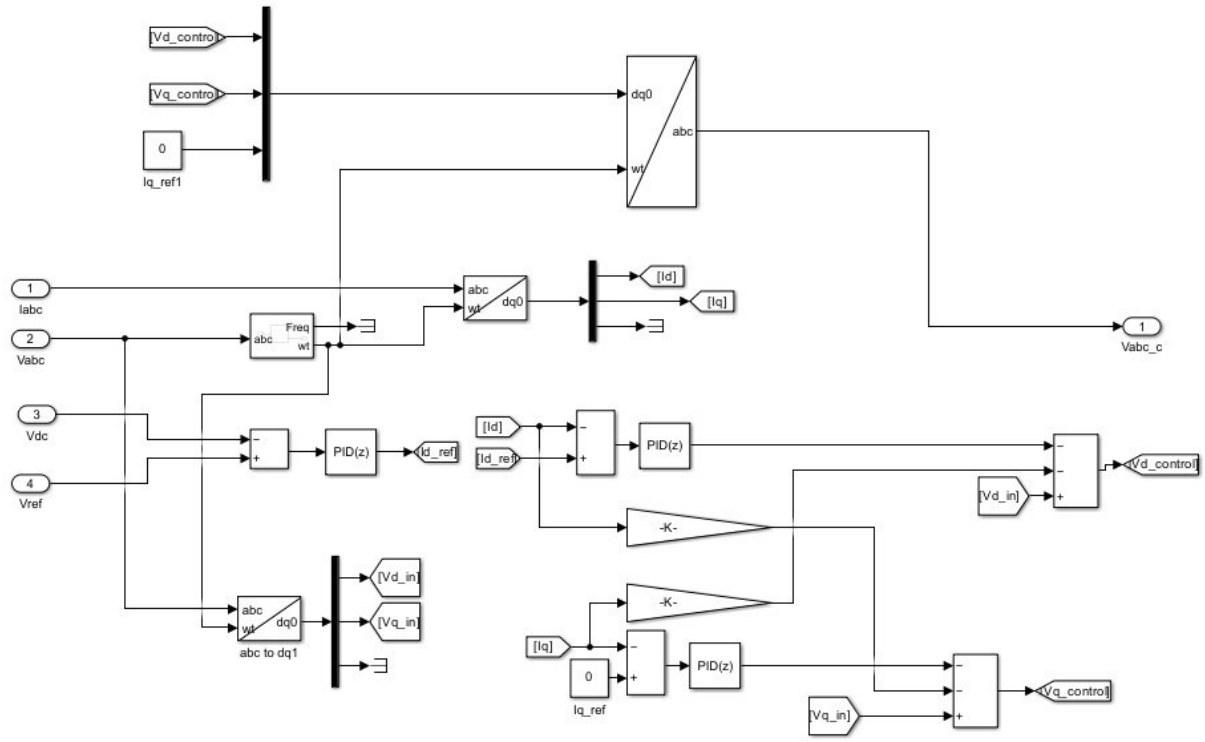

Figure A. 2 Simulation model of Three phase controlled rectifier

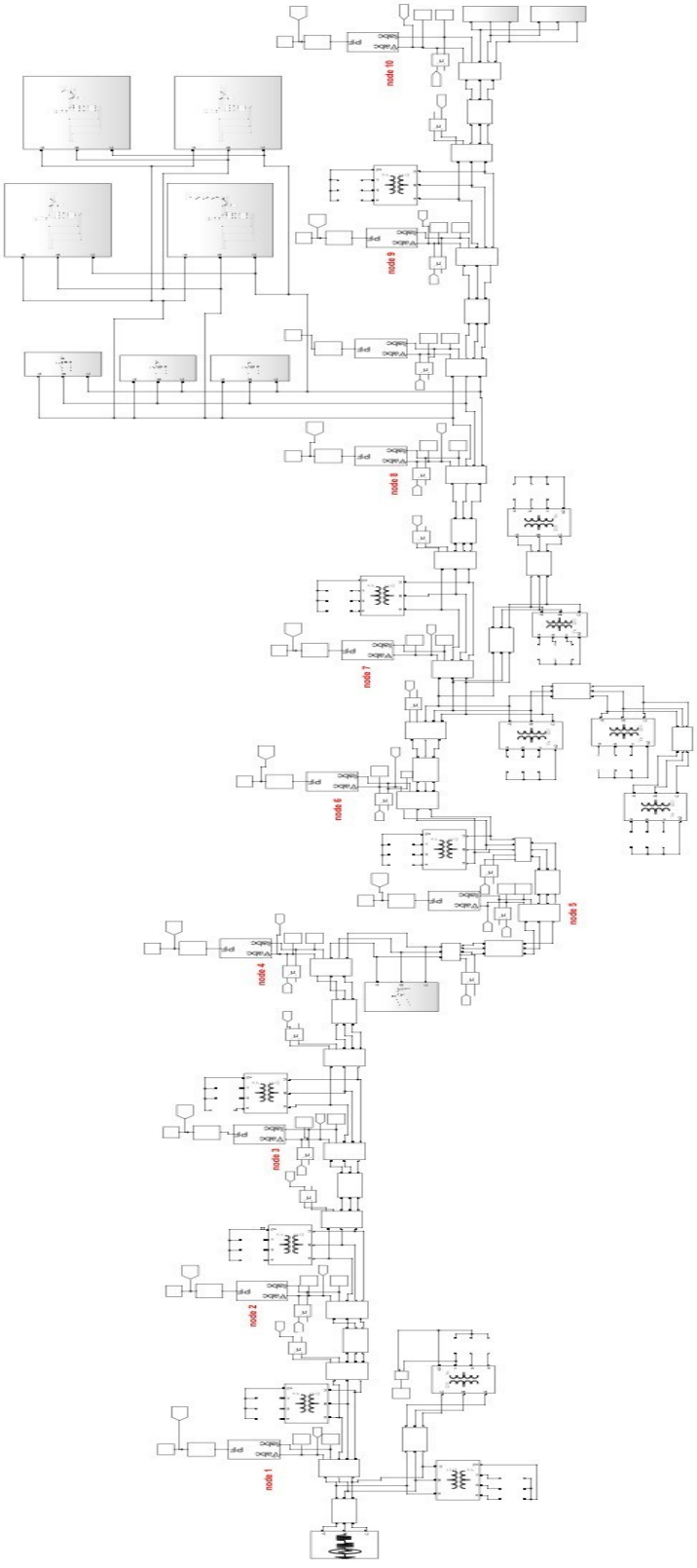

Figure A. 3 Overall simulation model of Sanepa Feeder

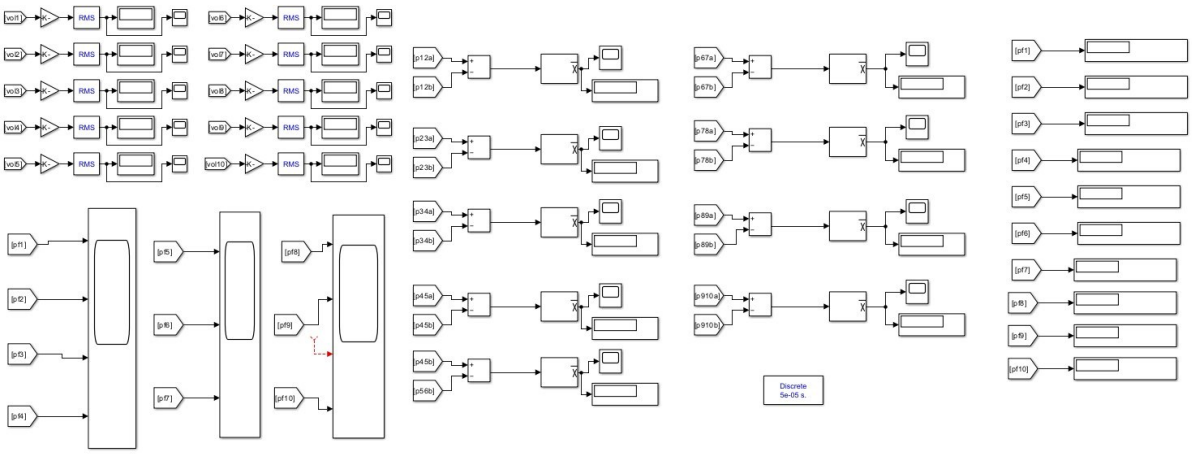

Figure A. 4 Measurement block of overall simulink model

Appendix B: Script

```
function ref = fcn(CV, CC,T, SOC)
persistent ref1 n
if isempty(ref1)
   ref1 = 0 ;
end
if isempty(n)
   n = 0 ;
end
if (T>n*0.000002) % sample time is 0.02s
   n=n+1;
   if SOC < 80.0
      ref1 = CC ;
   elseif SOC > 80.0
      ref1 = CV ;
   end
end
ref = ref1;
```

Appendix C: Table

Table A. 1 Data assumptions according to size of transformer

S (kVA)	%Z	X/R
100	4.0	5
200	4.0	5
250	4.5	5
300	4.5	5
500	5.0	5

Table A. 2 Base value calculation for various size of transformer

S (kVA)	S (VA)	Zbase HV (Ω)	Zbase LV (Ω)
100	100000	1210	1.6
200	200000	605	0.8
250	250000	484	0.64
300	300000	404	0.533
500	500000	242	0.32

Table A. 3 Series impedence calculation for various size of transformer

S (kVA)	Zpu	Rtotal_pu	Xtotal_pu	R1=R2 (pu)	L1=L2 (pu)
100	0.04	0.00784	0.0392	0.00392	0.0196
200	0.04	0.00784	0.0392	0.00392	0.0196
250	0.045	0.00882	0.0441	0.00441	0.0221
300	0.045	0.00882	0.0441	0.00441	0.0221
500	0.05	0.0098	0.049	0.0049	0.0245

Appendix D: Curves

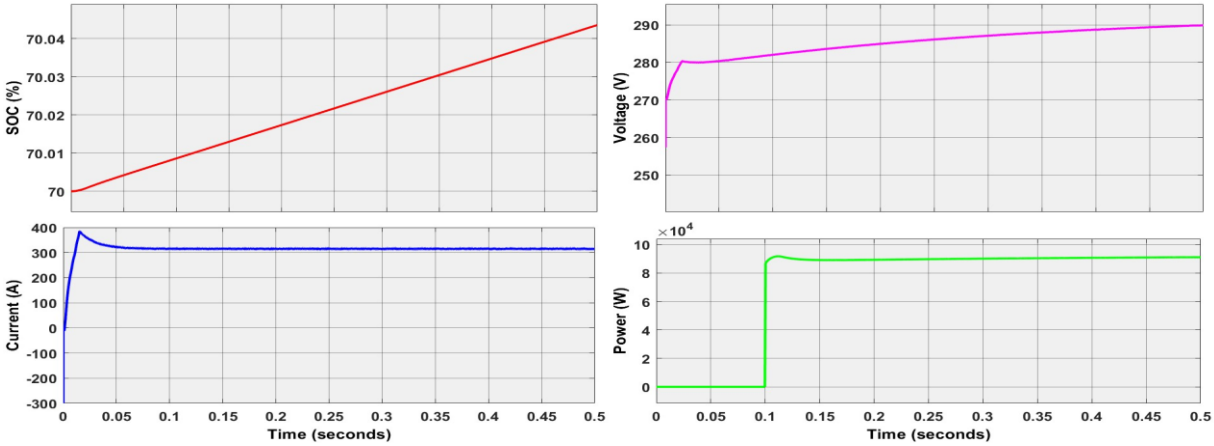

Figure A. 5 Performance waveforms of 90kW (315A) - Sajha Yatayat

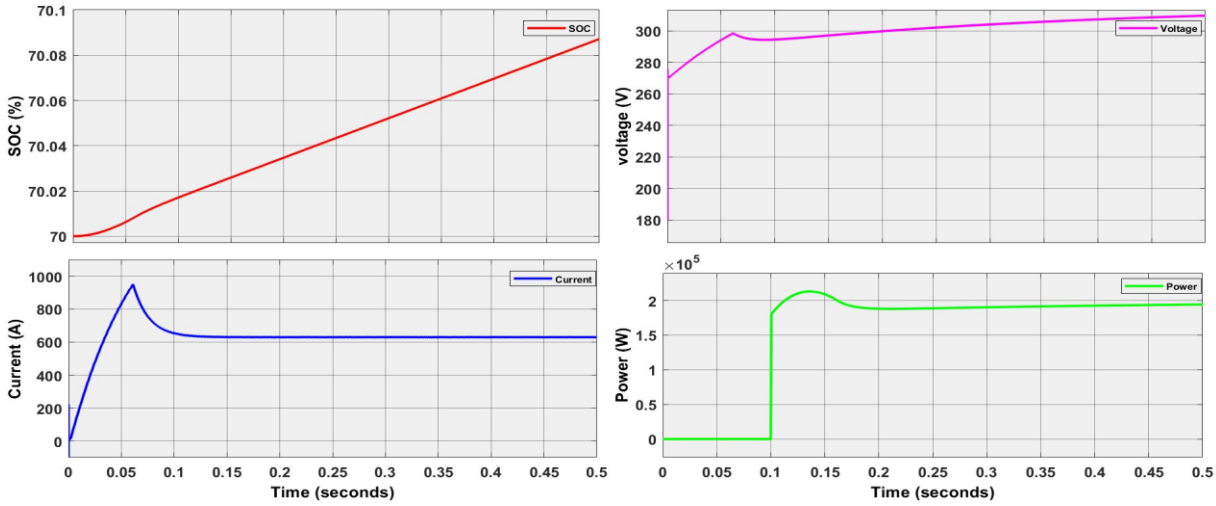

Figure A. 6 Performance waveforms of 180kW (630A) - Sajha Yatayat

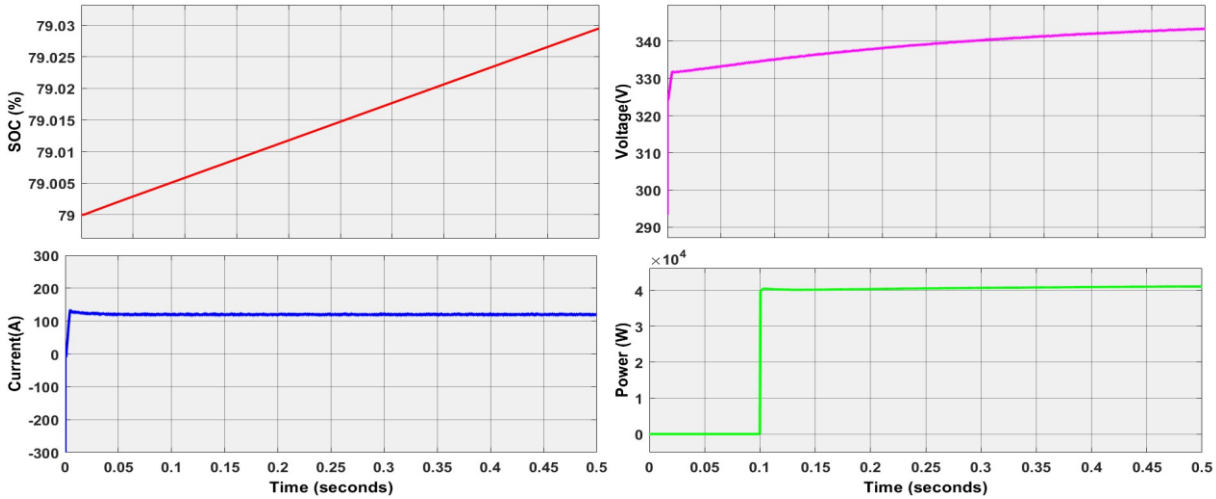

Figure A. 7 Performance waveforms of 40kW (120A) – BYD

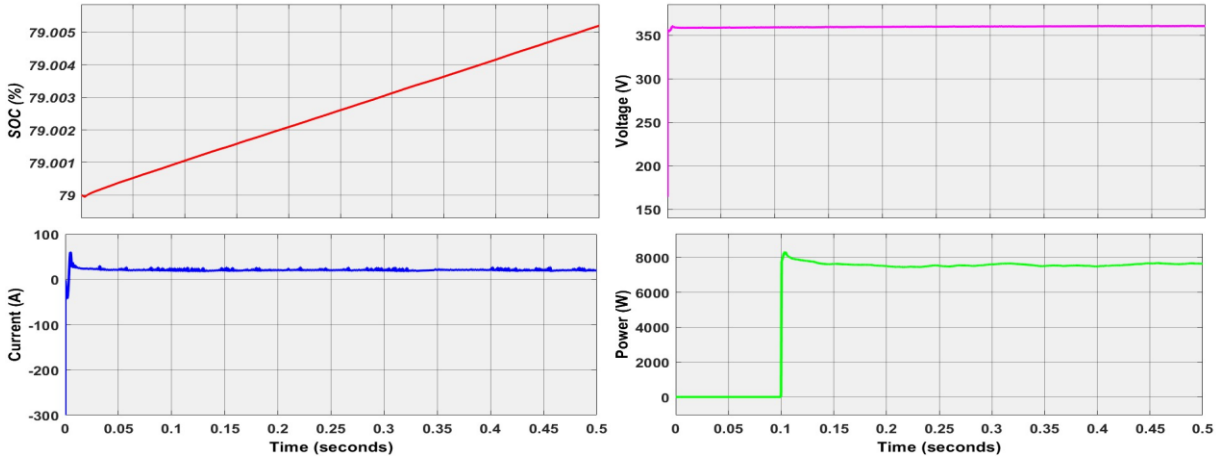

Figure A. 8 Performance waveforms of 7.3kW (32A) – Hyundai

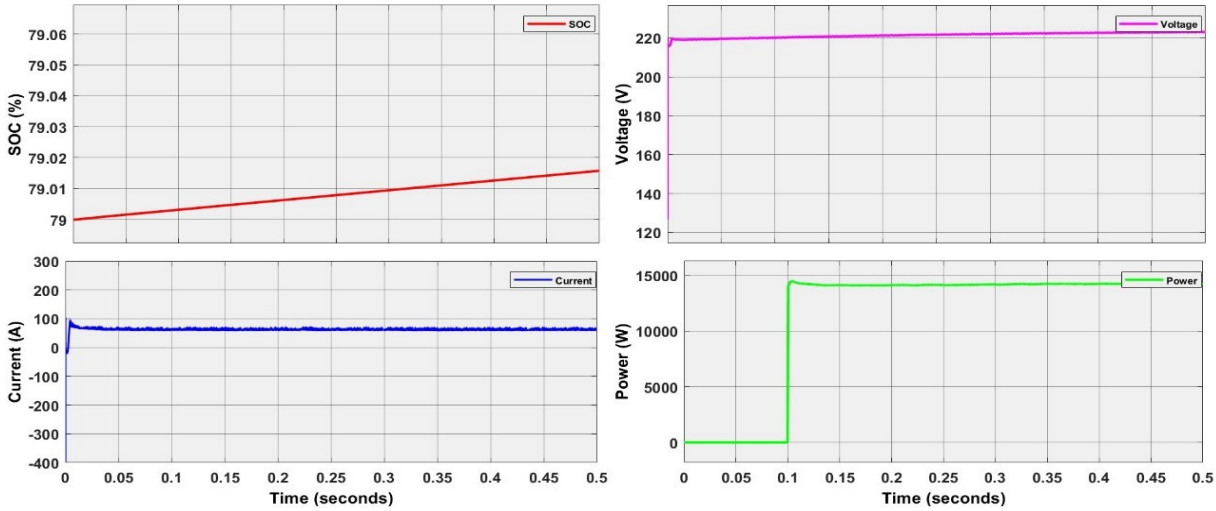

Figure A. 9 Performance waveforms of 14kW (64A) – MG

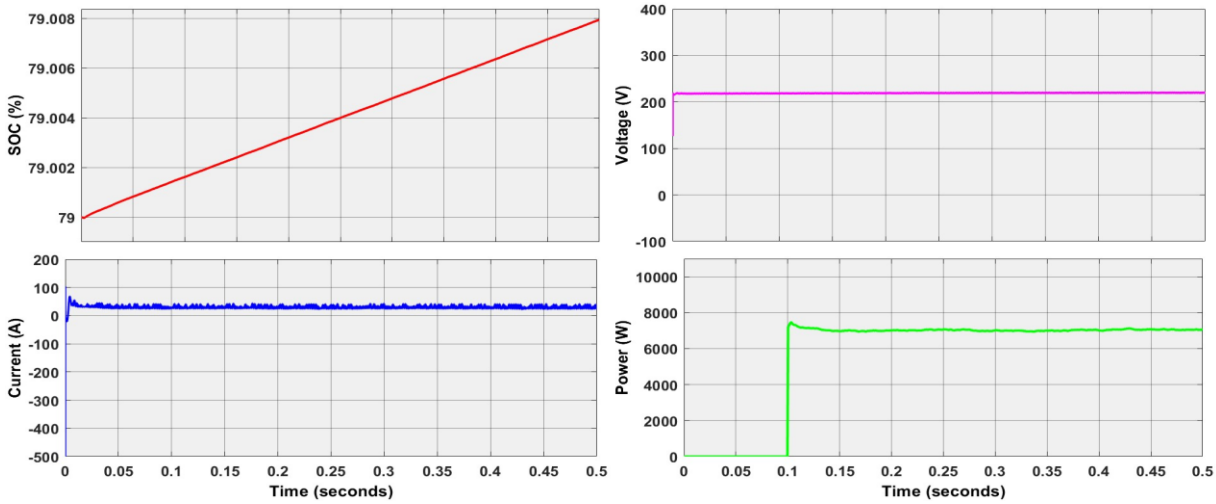

Figure A. 10 Performance waveforms of 7kW (32A) - MG

Notifications

[IOEGC17] Editor Decision

2025-12-04 02:51 PM

Om Bikram Shah:

We have reached a decision regarding your submission to 17th IOE Graduate Conference, "Impact Analysis of Electric Vehicle (EV) Charging on Medium Voltage Distribution Feeder Network (Sanepa Feeder)".

Our decision is to: Accept Submission (minor revisions required)

Reviewer's comments:
Overall, the paper is of good quality; however, the figures need improvement to ensure that all annotations are clearly readable.

With Warm Regards,
IOEGC-17 Editorial Team

Om

EV impact - revised for ai and plag check.pdf

Tribhuvan University

Document Details

Submission ID
trn:oid:::3117:536659456

Submission Date
Dec 5, 2025, 8:15 AM GMT+5:45

Download Date
Dec 5, 2025, 8:17 AM GMT+5:45

File Name
EV impact - revised for ai and plag check.pdf

File Size
5.2 MB

70 Pages

15,747 Words

77,261 Characters

7% Overall Similarity

The combined total of all matches, including overlapping sources, for each database.

Match Groups

103 Not Cited or Quoted 7%
Matches with neither in-text citation nor quotation marks

0 Missing Quotations 0%
Matches that are still very similar to source material

0 Missing Citation 0%
Matches that have quotation marks, but no in-text citation

0 Cited and Quoted 0%
Matches with in-text citation present, but no quotation marks

Top Sources

5% Internet sources
5% Publications
0% Submitted works (Student Papers)

Integrity Flags

1 Integrity Flag for Review

Replaced Characters
8 suspect characters on 3 pages
Letters are swapped with similar characters from another alphabet.

Our system's algorithms look deeply at a document for any inconsistencies that would set it apart from a normal submission. If we notice something strange, we flag it for you to review.

A Flag is not necessarily an indicator of a problem. However, we'd recommend you focus your attention there for further review.

Match Groups

- **103** Not Cited or Quoted 7%
  Matches with neither in-text citation nor quotation marks
- **0** Missing Quotations 0%
  Matches that are still very similar to source material
- **0** Missing Citation 0%
  Matches that have quotation marks, but no in-text citation
- **0** Cited and Quoted 0%
  Matches with in-text citation present, but no quotation marks

Top Sources

5% Internet sources
5% Publications
0% Submitted works (Student Papers)

Top Sources

The sources with the highest number of matches within the submission. Overlapping sources will not be displayed.

1	Internet	www.researchgate.net <1%
2	Publication	M.A. Rahman, T.S. Radwan, A.M. Osheiba, A.E. Lashine. "Analysis of current contr... <1%
3	Internet	epdf.pub <1%
4	Internet	vsip.info <1%
5	Internet	www.preprints.org <1%
6	Internet	www.jetir.org <1%
7	Publication	Mahesh Kumar Mishra. "Power Quality in Power Distribution Systems - Concepts ... <1%
8	Publication	Rameshchandra, Gupta Vinodkumar. "Novel technique for improving power quali... <1%
9	Publication	Arindam Ghosh, Gerard Ledwich. "Power Quality Enhancement Using Custom Po... <1%
10	Publication	J. C. Das. "Power System Harmonics and Passive Filter Designs", Wiley, 2015 <1%

11 Publication

Xiaoping He, Shuo Jiang, Yuxuan Yu, Siyi Su. "Impact of novel infrastructure inves... <1%

12 Internet

www.mdpi.com <1%

13 Publication

S.P. Gawande, M.R. Ramteke. "Current Controlled PWM for Multilevel Voltage-Sou... <1%

14 Publication

Amir A. Imam, R. Sreerama Kumar, Yusuf A. Al-Turki. "Modeling and Simulation of... <1%

15 Publication

Fritsche Barajas, Samuel. "Design and Implementation of a Medium Voltage Conv... <1%

16 Publication

Surajit Chattopadhyay, Madhuchhanda Mitra, Samarjit Sengupta. "Electric Power ... <1%

17 Internet

blog.smowcode.com <1%

18 Internet

research.riphah.edu.pk <1%

19 Internet

dspace.upt.ro <1%

20 Publication

Das, Byomakesh. "Novel Control and Harmonics Impact of PV Solar Farms", The U... <1%

21 Publication

S. Kannadhasan, R. Nagarajan, Alagar Karthick, V. Kumar Chinnaiyan. "Technolog... <1%

22 Internet

mdpi-res.com <1%

23 Internet

lte.techfak.uni-erlangen.de <1%

24 Publication

Ashutosh K. Giri, Sabha Raj Arya, Rakesh Maurya, B. Chitti Babu. "Mitigation of po... <1%

25 Internet
www.techscience.com <1%

26 Internet
ijpeds.iaescore.com <1%

27 Internet
repqj.com <1%

28 Internet
slideplayer.biz.tr <1%

29 Internet
slideplayer.com <1%

30 Internet
wiredspace.wits.ac.za <1%

31 Internet
www.journal.esrgroups.org <1%

32 Internet
www.mautc.psu.edu <1%

33 Internet
bura.brunel.ac.uk <1%

34 Internet
ijrti.org <1%

35 Internet
redpitaya-knowledge-base.readthedocs.io <1%

36 Publication
Khan, Md. Abdesh Shafiel Kafiey. "A wavelet based speed controller for interior p... <1%

37 Publication
Mohd Rizwan Khalid, M. S. Jamil Asghar, Mohammad Saad Alam, Salman Hameed,... <1%

38 Publication
S.Z. Djokic, J.V. Milanovic, D.S. Kirschen. "Sensitivity of AC Coil Contactors to Volta... <1%

39 Internet
assets.researchsquare.com <1%

40 Internet
utpedia.utp.edu.my <1%

41 Internet
www.csus.edu <1%

42 Publication
BOR-REN LIN, RICHARD G. HOFT. "ANALYSIS OF POWER CONVERTER CONTROL USI... <1%

43 Publication
Jian-Wen Zhao, Tao He, Cheng-Ming Liu, Ke Li. "Travelling Wave Fault Location for... <1%

44 Publication
Martin Rosenberger, Manfred Pl�chl, Klaus Six, Johannes Edelmann. "The Dynam... <1%

45 Internet
docplayer.fi <1%

46 Internet
www.modishproject.com <1%

47 Publication
Çetin, Alper. "Design and Implementation of a Voltage Source Converter Based St... <1%

48 Publication
B.N. Singh, P. Rastgoufard. "A new topology of active filter to correct power-facto... <1%

49 Publication
J. Mahdavi, M. Ehsani. "Power System Harmonic Control", Wiley, 1999 <1%

50 Publication
Rahul Raman, Pradip Kumar Sadhu, Ritesh Kumar, Shriram Srinivasarangan Rang... <1%

51 Publication
Zine Ghemari, Salah Belkhiri, Salima khaoula Reguieg. "Improving the Accuracy o... <1%

52 Internet
hdl.handle.net <1%

53 Publication

Chandwani, Hina B.. "Analysis, design, simulation and implementation of DSP bas... <1%

54 Publication

J.C. Das. "Power System Analysis - Short-Circuit Load Flow and Harmonics", CRC Pr... <1%

55 Publication

Singh, Siddhartha Anirban. "Design and Implementation of a Single Phase Modifi... <1%